

# The DODO Survey II: A Gemini Direct Imaging Search for Substellar and Planetary Mass Companions around Nearby Equatorial and Northern Hemisphere White Dwarfs

E. Hogan,<sup>1,2</sup> M.R. Burleigh,<sup>1</sup> and F.J. Clarke<sup>3</sup>

<sup>1</sup>*Department of Physics and Astronomy, University of Leicester, University Road, Leicester, LE1 7RH, UK*

<sup>2</sup>*Gemini Observatory, Casilla 603, La Serena, Chile*

<sup>3</sup>*Department of Astrophysics, Denys Wilkinson Building, University of Oxford, Keble Road, Oxford, OX1 3RH, UK*

26 October 2021

## ABSTRACT

The aim of the Degenerate Objects around Degenerate Objects (DODO) survey is to search for very low mass brown dwarfs and extrasolar planets in wide orbits around white dwarfs via direct imaging. The direct detection of such companions would allow the spectroscopic investigation of objects with temperatures much lower ( $< 500$  K) than the coolest brown dwarfs currently observed. These ultra-low mass substellar objects would have spectral types  $> T8.5$  and so could belong to the proposed Y dwarf spectral sequence. The detection of a planet around a white dwarf would prove that such objects can survive the final stages of stellar evolution and place constraints on the frequency of planetary systems around their progenitors (with masses between  $1.5 - 8 M_{\odot}$ , i.e., early B to mid F). This paper presents the results of a multi-epoch  $J$  band common proper motion survey of 23 nearby equatorial and northern hemisphere white dwarfs. We rule out the presence of any common proper motion companions, with limiting masses determined from the completeness limit of each observation, to 18 white dwarfs. For the remaining five targets, the motion of the white dwarf is not sufficiently separated from the non-moving background objects in each field. These targets require additional observations to conclusively rule out the presence of any common proper motion companions. From our completeness limits, we tentatively suggest that  $\lesssim 5\%$  of white dwarfs have substellar companions with  $T_{\text{eff}} \gtrsim 500$  K between projected physical separations of  $60 - 200$  AU.

**Key words:** stars: white dwarfs; planetary systems; low mass, brown dwarfs; imaging.

## 1 INTRODUCTION

Directly imaging the extrasolar planets found in orbit around solar type stars is difficult as these faint companions are too close to their bright parent stars. As this paper was being finalised, Kalas et al. (2008) announced the discovery of a directly imaged  $\sim 3 M_{\text{Jup}}$  extrasolar planet with a projected physical separation of 119 AU in orbit around the A-type star Fomalhaut. On the same day, Marois et al. (2008) announced the discovery of three directly imaged companions around the A-type star HR8799 with likely masses between  $5 - 13 M_{\text{Jup}}$  and projected physical separations of 24, 38 and 68 AU. However, coronagraphy and adaptive optics were needed to detect these faint extrasolar planets. Another, perhaps simpler, solution to the problems of contrast and resolution is to instead target intrinsically faint stars. For example, many groups are already

searching for planetary mass companions<sup>1</sup> in orbit around young, low mass stars and brown dwarfs (e.g., Chauvin et al. 2003; Neuhäuser et al. 2003). Any planetary mass companions found in orbit around these young stars will have

<sup>1</sup> We make the distinction between very low mass brown dwarfs and massive extrasolar planets by formation mechanism rather than mass, since the mass distributions of these two types of object likely overlap. For example, the  $9 M_{\text{Jup}}$  transiting object HAT-P-2b is too dense to be a brown dwarf (Baraffe et al. 2008), while the free floating objects with masses of the order of a few Jupiter masses that have been found in young clusters possibly formed in the same manner as stars. Indeed, some authors insist that the IAU distinction between these two populations, based on mass alone, has no valid foundation (Chabrier et al. 2008). Therefore, throughout this paper we prefer to use the term “planetary mass object” to refer to any body at or below the deuterium burning limit ( $13 - 14 M_{\text{Jup}}$ ), since the evolutionary history of any companions discovered with these masses is uncertain.

relatively high luminosities, since planetary mass objects cool continuously from the moment they form. Famously, a  $\sim 4 \pm 1 M_{\text{Jup}}$  (Ducourant et al. 2008) companion to the  $\sim 25 M_{\text{Jup}}$  brown dwarf member of the TW Hydrae association 2MASSW J1207334 – 393254 (2M1207) was imaged by Chauvin et al. (2004, 2005). However, Lodato et al. (2005) argue that 2M1207Ab more likely formed as a binary brown dwarf system, since the core accretion model, thought to be the most likely formation mechanism for gas giants like those in the Solar System, is unable to account for the formation of 2M1207b.

An alternative approach, rather than looking at the bright, early part of a planet’s life, is to look at the faint, late part of a star’s life. White dwarfs are intrinsically faint stars and can be up to 10,000 times less luminous than their main sequence progenitors, significantly enhancing the contrast between any companion and the white dwarf. In addition, any companion that avoids direct contact with the red giant envelope as the main sequence progenitor evolves into a white dwarf will migrate outwards as mass is lost from the central star by a maximum factor of  $M_{\text{MS}}/M_{\text{WD}}$  (Jeans 1924). This increases the projected physical separation between the companion and the white dwarf, substantially increasing the probability of obtaining a ground based direct image of a planetary mass companion. The evolution of planetary systems during the post-main sequence phase is discussed in more detail by Duncan & Lissauer (1998), Burleigh, Clarke & Hodgkin (2002), Debes & Sigurdsson (2002) and Villaver & Livio (2007).

The direct detection of a planetary mass companion in orbit around a white dwarf would allow the spectroscopic investigation of very low mass objects much cooler ( $< 500$  K) than previously found. The coolest known brown dwarfs, ULAS J003402.77 – 005206.7 (Warren et al. 2007) and CF-BDS J005910.90 – 011401.3 (Delorme et al. 2008), have effective temperatures of  $600 < T_{\text{eff}} < 700$  K and spectral types of T8.5. The letter Y has been suggested for the next, cooler, spectral type (Kirkpatrick 2005). Any planetary mass companions directly detectable around old ( $> 2$  Gyr) white dwarfs could well belong to this class, regardless of formation mechanism (Zuckerman & Song 2008). Such a discovery would help provide constraints on models for the evolution of planets and planetary systems during the final stages of stellar evolution. In addition, the age of any substellar and planetary mass companions discovered in such a system can be estimated using the white dwarf cooling age and the mass and the lifetime of the main sequence progenitor, providing model-free benchmark estimates of their mass and luminosity, which could be used to test evolutionary models (Pinfield et al. 2006). Radial velocity searches have concentrated mainly on stars with spectral types between mid F and M, since the faster rotation and increased activity of early B, A and mid F type stars broadens the low number of absorption lines in their spectra. As a result, it is difficult to accurately measure the Doppler shift of stars with these earlier spectral types. However, new methods in manipulating the measurements acquired when using the radial velocity technique has allowed planetary mass companions to be found around stars with spectral types of A and F (e.g., Galland et al. 2005). Nevertheless, as the  $1.5 - 8 M_{\odot}$  progenitor stars of white dwarfs have spectral types of early

B, A and mid F, searching for planetary mass companions in orbit around white dwarfs allows the examination of a currently inadequately explored region of parameter space, supplying new information on the frequency and mass distribution of extrasolar planets around intermediate mass main sequence stars.

A number of extrasolar planets have been discovered around evolved giant stars using the radial velocity technique, e.g., HD 11977 (G5 III; Setiawan et al. 2005), HD 13189 (K2 II; Hatzes et al. 2005) and  $\beta$  Gem (K0 III; Hatzes et al. 2006; Reffert et al. 2006). These stars have entered the red giant phase of stellar evolution, proving that planets can survive the early stages of the RGB phase. Evolved giant stars are significantly more massive than the Sun, so their progenitors were likely to be A or B type stars (see Table 6 of Hatzes et al. 2006). The companions all have masses significantly larger than Jupiter, implying that significantly more massive planets are formed around these intermediate mass stars than around lower mass stars (Lovis & Mayor 2007). In fact, both Lovis & Mayor (2007) and Johnson et al. (2007) suggest that intermediate mass stars are more likely to host extrasolar planets of all masses than solar mass stars.

Up to three white dwarfs are known to be wide companions to stars hosting extrasolar planets. The bright ( $V = 11$  mag), well studied white dwarf WD 1620 – 391 (CD–38°10980) was known to be a common proper motion companion to the solar type star HD 147513 (Wegner 1973) before a planet, with a minimum mass,  $M_{\text{p}} \sin i = 1.21 M_{\text{Jup}}$  and an orbital radius of 1.32 AU, was discovered in orbit around the latter (Mayor et al. 2004). Since WD 1620 – 391 and the parent star are separated by  $\sim 5360$  AU, it is highly unlikely that the evolution of the main sequence progenitor of the white dwarf affected the mass or the orbit of HD 147513b. It has been suggested that the faint companions to two other planet hosting stars are also white dwarfs. The planet in orbit around Gliese 86 has a minimum mass,  $M_{\text{p}} \sin i = 4.01 M_{\text{Jup}}$  and an orbital period of 15.8 days (Queloz et al. 2000), while the likely white dwarf companion has a mass between  $0.48 \leq M \leq 0.62 M_{\odot}$  and an orbital radius of  $\sim 20$  AU (Mugrauer & Neuhäuser 2005; Lagrange et al. 2006). The possible effects of the evolution of the main sequence progenitor on the mass and the orbit of the planet are discussed by Desidera & Barbieri (2007). The planet in orbit around HD 27442 ( $\epsilon$  Ret) has a minimum mass,  $M_{\text{p}} \sin i = 1.28 M_{\text{Jup}}$  and an orbital radius of 1.18 AU (Butler et al. 2001). The white dwarf companion (Raghavan et al. 2006; Chauvin et al. 2006), currently separated from HD 27442 by  $\sim 240$  AU, was recently confirmed from an analysis of its optical and infrared (IR) spectrum (Mugrauer et al. 2007; Chauvin et al. 2007).

The discovery of metal rich dust disks in close orbits around white dwarfs may indicate the existence of old, rocky planetary systems, suggesting that even terrestrial planets and asteroids can survive the final stages of stellar evolution. The first dust disk was discovered around the DAZ white dwarf G 29 – 38 (WD 2326 + 049) from the identification of a large IR excess in its spectrum at wavelengths between  $2 - 5 \mu\text{m}$  (Zuckerman & Becklin 1987b). This IR excess was initially attributed to a spatially unresolved,  $T_{\text{eff}} = 1200 \pm 200$  K brown dwarf companion to the white dwarf. However, subsequent measurements showed that the

blackbody-like IR excess was due to a dust disk rather than a brown dwarf (Tokunaga, Becklin & Zuckerman 1990). A mid-IR (MIR) spectrum of G 29 – 38, obtained by the Spitzer Space Telescope, shows a strong emission feature in the spectrum between 9–11  $\mu\text{m}$ , which indicates the presence of silicates ( $\text{SiO}_4$ ) in the dust disk (Reach et al. 2005). Eight additional white dwarfs are now known to have dust disks in orbit around them: GD 362 ( $T_{\text{eff}} = 9740$  K; Becklin et al. 2005; Kilic et al. 2005), GD 56 ( $T_{\text{eff}} = 14400$  K; Kilic et al. 2006), WD 1150 – 153 ( $T_{\text{eff}} = 12800$  K; Kilic & Redfield 2007), WD 2115 – 560 ( $T_{\text{eff}} = 9700$  K; von Hippel et al. 2007), GD 40 ( $T_{\text{eff}} = 15200$  K; Jura, Farihi & Zuckerman 2007), GD 133 ( $T_{\text{eff}} = 12200$  K; Jura et al. 2007), PG 1015 + 161 ( $T_{\text{eff}} = 19300$  K; Jura et al. 2007) and G 166 – 58 ( $T_{\text{eff}} = 7390$  K; Farihi et al. 2008). The generally accepted origin of the material in these dust disks is from the tidal disruption of an asteroid that had strayed within the Roche lobe radius of the white dwarf after its orbital radius was altered during the AGB phase of stellar evolution (Graham et al. 1990; Debes & Sigurdsson 2002; Jura 2003). In addition to these dust disks, there have been metal rich gas disks found in orbit around 2 hotter DAZ white dwarfs; SDSS J122859.93 + 104032.0 ( $T_{\text{eff}} = 22292$  K; Gänsicke et al. 2006) and SDSS J104341.53 + 085558.2 ( $T_{\text{eff}} = 18330$  K; Gänsicke, Marsh & Southworth 2007). These gas disks could also indicate the presence of old planetary systems, since it is likely that the hot white dwarfs caused the dust in the disk to sublimate. The fraction of known single DAZ white dwarfs with IR excesses, which can be attributed to a dust disk, is 14% (Kilic et al. 2006). In addition, Jura (2006) argues that  $> 7\%$  of white dwarfs possess asteroid belts similar to that of the Solar System, and by implication, remnant planetary systems.

The first search for low mass substellar companions to white dwarfs was conducted by Probst (1983), who measured the IR magnitudes of  $\sim 100$  white dwarfs to determine whether any excess emission was present. No companions were found during this survey. Subsequently, a number of groups unsuccessfully attempted to detect substellar companions to white dwarfs using the same method (e.g., Shipman 1986; Zuckerman & Becklin 1987a). The first confirmed substellar companion to a white dwarf was discovered in 1988 around the DA white dwarf GD 165 (Becklin & Zuckerman 1988). Over 15 years later, a second brown dwarf companion was found in orbit around GD 1400 (Farihi & Christopher 2004; Dobbie et al. 2005). More recently, radial velocity measurements revealed a brown dwarf companion in a close ( $\sim 116$  minutes) orbit around WD 0137 – 349 (Maxted et al. 2006), while its spectral type (L8) was later determined from near-IR (NIR) spectroscopy (Burleigh et al. 2006). The L dwarf companion fraction, determined from a wide field, proper motion, NIR search for wide substellar companions to 347 white dwarfs, is estimated to be  $< 0.5\%$  (Farihi et al. 2005).

The recent discovery of an extrasolar planet around the post-red giant star V 391 Pegasi proves that planetary mass companions with an initial orbital radius outside the maximum radius of the red giant envelope can survive the RGB phase of stellar evolution. The planet was discovered from the periodic variation in the precise timing measurements of V 391 Pegasi’s extremely stable, short period pulsations (Silvotti et al. 2007). It has a minimum

mass,  $M_p \sin i \sim 3.2 M_{\text{Jup}}$ , an orbital radius of  $\sim 1.7$  AU and an estimated age of  $\sim 10$  Gyr. Strong evidence for the existence of a planetary mass companion to the DAV white dwarf GD 66 has been recently found from the periodic variation in the precise timing measurements of GD 66’s extremely stable non-radial pulsations (Mullally et al. 2008). While current measurements suggest that this companion has a minimum mass,  $M_p \sin i \sim 2.11 M_{\text{Jup}}$  and an orbital radius of  $\sim 2.356$  AU, further observations, to cover the entire orbit of the companion, are now required.

In Burleigh et al. (2008) we reported limits on planetary mass companions to the nearest single white dwarf, vMa 2. Preliminary results and progress reports from the Degenerate Objects around Degenerate Objects (DODO) survey have been published previously (Clarke & Burleigh 2004; Burleigh, Hogan & Clarke 2006; Hogan, Burleigh & Clarke 2007). In this paper we report further extensive results of the DODO survey; a NIR direct imaging search for substellar and planetary mass common proper motion companions in wide orbits around nearby white dwarfs.

## 2 TARGET SELECTION

The ability to directly image an extrasolar planet in orbit around a white dwarf will depend on the apparent magnitude of the planet, which in turn depends on its absolute magnitude and distance from the Earth. The absolute magnitude of the planet is determined from its intrinsic luminosity, which is dependant primarily on the age and the mass of the planet, since it will cool continuously from the moment it formed. The age of an extrasolar planet found in orbit around a white dwarf equals the sum of the main sequence progenitor lifetime and the white dwarf cooling age. Using this age and the distance to the white dwarf, Burleigh et al. (2002) used evolutionary models for cool brown dwarfs and extrasolar planets (Burrows et al. 1997) to make initial predictions of the IR magnitudes of planetary mass companions around white dwarfs. The results published in this paper use the more recent “COND” evolutionary models of Baraffe et al. (2003). These models assume irradiation effects from the parent star on the planet are negligible and predict that a  $5 M_{\text{Jup}}$  planet with an age of  $\sim 2$  Gyr will have an apparent magnitude of  $J \sim 24$  mag at 10 pc. This magnitude is comparable with the expected sensitivity of a one hour exposure acquired using an 8m telescope. Brighter companions such as massive brown dwarfs and M dwarfs should easily be detected. Indeed, these more luminous objects would have already been detected in previous IR studies (e.g., Farihi et al. 2005) and in 2MASS data.

Lower mass planets could be more easily detected around younger white dwarfs, since these companions would be brighter than their older counterparts. In addition, fainter, and therefore lower mass, companions could be more easily detected around nearby white dwarfs compared to more distant targets. Nearby white dwarfs are also more likely to have large proper motions, which require a smaller baseline between the observations of the two epochs. An initial sample of  $\sim 40$  targets, with total ages (main sequence progenitor lifetime plus the white dwarf cooling age)  $< 4$  Gyr and distances within  $\sim 20$  pc, were selected from the cata-

**Table 1.** Parameters of the 23 equatorial and northern hemisphere white dwarfs in the DODO survey

White Dwarf	Name	Sp. Class	$\mu$ [m''/yr]	$\theta$ [m''/yr]	$d$ [pc]	$T_{\text{eff}}$ [K]	$\log g$	$M_{\text{WD}}$ [ $M_{\odot}$ ]	$t_{\text{WD}}$ [Gyr]	$M_{\text{MS}}$ [ $M_{\odot}$ ]	$t_{\text{MS}}$ [Gyr]	$t_{\text{tot}}$ [Gyr]	R
0115 + 159	LHS 1227	DQ	-20 <sup>1</sup>	-647 <sup>1</sup>	15.41 <sup>2</sup>	9050	8.19	0.69	1.02*	3.0	0.63	1.7	3
0148 + 467	GD 279	DA	1 <sup>4</sup>	124 <sup>4</sup>	15.85 <sup>4</sup>	13990	7.89	0.53	0.21*	1.8	2.26	2.5	5
0208 + 396	G 74-7	DAZ	1031 <sup>1</sup>	-497 <sup>1</sup>	16.72 <sup>2</sup>	7310	8.01	0.60	1.38	2.3	1.20	2.6	6
0341 + 182	Wolf 219	DQ	415 <sup>1</sup>	-1125 <sup>1</sup>	19.01 <sup>2</sup>	6510	7.99	0.57	1.79*	2.1	1.54	3.3	3
0435 - 088	L 879-14	DQ	243 <sup>1</sup>	-1555 <sup>1</sup>	9.51 <sup>2</sup>	6300	7.93	0.53	1.79*	1.8	2.26	4.1	3
0644 + 375	G 87-7	DA	-226 <sup>4</sup>	-936 <sup>4</sup>	15.41 <sup>4</sup>	21060	8.10	0.54 <sup>7</sup>	0.07*	1.9	2.04	2.1	5
0738 - 172	L 745-46A	DZ	1147 <sup>1</sup>	-538 <sup>1</sup>	8.90 <sup>2</sup>	7710	8.09	0.63	1.45	2.6	0.95	2.4	6
0912 + 536	G 195-19	DCP <sup>a</sup>	-1086 <sup>1</sup>	-1125 <sup>1</sup>	10.28 <sup>2</sup>	7160	8.28	0.75	2.54	3.5	0.45	3.0	6
1055 - 072	LHS 2333	DC	-822 <sup>1</sup>	91 <sup>1</sup>	12.15 <sup>2</sup>	7420	8.42	0.85	3.01	4.2	0.27	3.3	6
1121 + 216	Ross 627	DA	-1040 <sup>1</sup>	-14 <sup>1</sup>	13.44 <sup>2</sup>	7490	8.20	0.72	1.76	3.2	0.53	2.3	6
1134 + 300	GD 140	DA	-147 <sup>4</sup>	-6 <sup>4</sup>	15.32 <sup>4</sup>	21280	8.55	0.96	0.20	5.0	0.17	0.37	8
1344 + 106	LHS 2800	DAZ	-871 <sup>9</sup>	-181 <sup>9</sup>	20.04 <sup>2</sup>	7110	8.10	0.65	1.67	2.7	0.82	2.5	6
1609 + 135	LHS 3163	DA	14 <sup>1</sup>	-551 <sup>1</sup>	18.35 <sup>2</sup>	9080	8.75	1.07	2.71	5.9	0.12	2.8	6
1626 + 368	Ross 640	DZ	-469 <sup>9</sup>	709 <sup>9</sup>	15.95 <sup>2</sup>	8640	8.03	0.60	1.02	2.3	1.20	2.2	6
1633 + 433	G 180-63	DAZ	218 <sup>1</sup>	-302 <sup>1</sup>	15.11 <sup>2</sup>	6650	8.14	0.68	2.28	2.9	0.67	3.0	6
1647 + 591	G 226-29	DAV	139 <sup>4</sup>	-292 <sup>4</sup>	10.97 <sup>4</sup>	12260	8.31	0.80	0.56*	3.8	0.35	0.91	10
1900 + 705	G 260-15	DAP <sup>b</sup>	105 <sup>9</sup>	479 <sup>9</sup>	12.99 <sup>2</sup>	12070	8.58	0.95	0.94	5.0	0.18	1.1	6
1953 - 011	G 92-40	DAP <sup>c</sup>	-442 <sup>1</sup>	-699 <sup>1</sup>	11.39 <sup>2</sup>	7920	8.23	0.74	1.63	3.4	0.47	2.1	6
2007 - 219	LTT 7983	DA	109 <sup>1</sup>	-313 <sup>1</sup>	18.22 <sup>11</sup>	9887	8.14	0.69	0.76*	3.0	0.63	1.4	12
2047 + 372	G 210-36	DA	160 <sup>1</sup>	149 <sup>1</sup>	18.16 <sup>11</sup>	14630	8.13	0.69	0.26*	3.0	0.63	0.89	13
2140 + 207	LHS 3703	DQ	-207 <sup>9</sup>	-658 <sup>9</sup>	12.52 <sup>2</sup>	8200	7.84	0.49	0.82*	1.5	3.56	4.4	3
2246 + 223	G 67-23	DA	580 <sup>9</sup>	13 <sup>9</sup>	19.05 <sup>2</sup>	10330	8.57	0.97	1.56	5.1	0.17	1.7	6
2326 + 049	G 29-38	DAZ <sup>d</sup>	-360 <sup>9</sup>	-302 <sup>9</sup>	13.62 <sup>2</sup>	11820	8.15	0.70	0.55	3.1	0.60	1.1	8

Columns:  $\mu$  and  $\theta$  are the R.A. and Dec components of the proper motion of the white dwarf, respectively, measured in milli arc seconds per year;  $d$  is the distance to the white dwarf, measured in parsecs;  $T_{\text{eff}}$  is the effective temperature of the white dwarf, measured in Kelvin;  $\log g$  is the log of the gravity of the white dwarf;  $M_{\text{WD}}$  is the mass of the white dwarf, measured in solar masses;  $t_{\text{WD}}$  is the cooling age of the white dwarf, measured in gigayears;  $M_{\text{MS}}$  is the mass of the main sequence progenitor, measured in solar masses, and is calculated using the IFMR of Dobbie et al. 2006;  $t_{\text{MS}}$  is the main sequence lifetime, measured in gigayears, and is calculated using Equation 2 (Wood 1992);  $t_{\text{tot}}$  is the total age of the white dwarf, measured in gigayears.

R = References, which refer to the  $T_{\text{eff}}$ ,  $\log g$ ,  $M_{\text{WD}}$  and  $t_{\text{WD}}$  columns. (1) Salim & Gould (2003), (2) van Alena, Lee & Hoffleit (1995), (3) Dufour, Bergeron & Fontaine (2005), (4) Perryman et al. (1997), (5) Bergeron, Saffer & Liebert (1992), (6) Bergeron, Leggett & Ruiz (2001), (7) Fontaine, Bergeron & Brassard (2007), (8) Liebert, Bergeron & Holberg (2005), (9) Bakos, Sahu & Németh (2002), (10) Gianninas, Bergeron & Fontaine (2005), (11) Holberg, Oswalt & Sion (2002), (12) Koester et al. (2001), (13) Giovannini et al. (1998), <sup>a</sup>Magnetic field strength,  $B = 100$  MG; rotation period,  $P = 1.3$  days (Wickramasinghe & Ferrario 2000), <sup>b</sup>Magnetic field strength,  $B = 320$  MG (Wickramasinghe & Ferrario 2000), <sup>c</sup>Magnetic field strength,  $B = 70$  kG; rotation period,  $P = 1.4418$  days. WD 1953 - 011 is also photometrically variable at the  $\sim 2\%$  level, an effect which is believed to be caused by a star spot (Brinkworth et al. 2005), <sup>d</sup>A dust disk is known to orbit this ZZ ceti white dwarf, \*The white dwarf cooling age was calculated using models from Fontaine, Brassard & Bergeron (2001).

logue of white dwarfs within 20pc Holberg et al. (2002). Of these targets, 23 equatorial and northern hemisphere white dwarfs (Table 1) are presented in this paper. The remaining southern hemisphere white dwarfs will be presented in an upcoming paper.

The cooling age of a white dwarf,  $t_{\text{WD}}$ , can be calculated using evolutionary models. When the cooling age was unavailable in the literature, models from Fontaine, Brassard & Bergeron (2001), which use  $T_{\text{eff}}$  and  $\log g$  values to calculate the cooling age, were used to estimate this value. The initial final mass relation (IFMR) determined by Dobbie et al. (2006), based on the measurements of a small number of white dwarfs found in young open clusters, was used to determine the mass of the main sequence progenitor,  $M_{\text{MS}}$ , from the mass of the white dwarf,  $M_{\text{WD}}$ . This linear IFMR is given as

$$M_{\text{WD}} = 0.133 M_{\text{MS}} + 0.289 \quad (1)$$

Recent observations of white dwarfs in older open clusters have placed constraints on the low mass end of the IFMR,

suggesting that this equation is valid down to white dwarf masses of  $0.54 M_{\odot}$  (Kalirai et al. 2008). The main sequence progenitor lifetime,  $t_{\text{MS}}$ , is estimated using the equation

$$t_{\text{MS}} = 10 \left( \frac{M_{\text{MS}}}{M_{\odot}} \right)^{-2.5} \quad (2)$$

where  $t_{\text{MS}}$  is measured in Gyr (Wood 1992).

### 3 OBSERVATIONS

Observations of the 23 equatorial and northern hemisphere white dwarfs (Table 2) were acquired in the  $J$  band primarily using Gemini North and *NIRI* between 2003 and 2005, while a small number of observations of equatorial targets were acquired in 2002, using Gemini South and *FLAMINGOS*. *NIRI* consists of a  $1024 \times 1024$  pixel ALADDIN-II array. When combined with the f/6 camera, *NIRI* supplies a pixel scale of  $0.117''$  pixel<sup>-1</sup> and a wide field of view of  $120'' \times 120''$ . *FLAMINGOS* consists of a  $2048 \times 2048$  pixel HAWAII-II

array. When combined with the f/16 camera, *FLAMINGOS* supplies a pixel scale of  $0.078'' \text{ pixel}^{-1}$  and a wide field of view of  $160'' \times 160''$ .

The science data were acquired using a dither pattern, which involved systematically offsetting the telescope, to allow the effective removal of the sky background. The total exposure time given in Table 2 was achieved by obtaining 60 second and 90 second individual exposures per dither position for *NIRI* and *FLAMINGOS*, respectively. The number of coadds acquired for each individual exposure was adjusted to avoid saturating the white dwarf. Unfortunately, on occasion, the requested exposure time of 1 hour was not always achieved. “Lamps on” dome flats were acquired by imaging a uniformly illuminated screen within the dome. “Lamps off” dome flats were acquired using the same method, except with no illumination of the screen. These dome flats were used for the calibration of the *NIRI* science data. High and low twilight flats were acquired for the calibration of the *FLAMINGOS* data. Short dark frames were also acquired to help with the identification of bad pixels.

#### 4 DATA REDUCTION

All the data acquired for the DODO survey were reduced using the Image Reduction and Analysis Facility (IRAF; Tody 1986) and the GEMINI package, versions 2.12.2a and 1.8, respectively. Raw *NIRI* images are in the form of multi-extension fits (MEF) files with most of the header information in the Primary Header Unit (PHU), “[0]” extension and the raw image data in the second, “[1]” extension. Raw *FLAMINGOS* images are in the form of single extension fits files. The NPREPARE and FPREPARE tasks in the GEMINI package were applied to all raw data acquired with *NIRI* and *FLAMINGOS*, respectively. These tasks add certain essential keywords to the header of each data file, allowing the subsequent data reduction tasks to be applied. In addition, the FPREPARE task converted all the *FLAMINGOS* images into MEF files. This made it possible for both the *NIRI* and the *FLAMINGOS* data to be reduced in a homogeneous manner, using the *NIRI* tasks in the GEMINI package.

For the reduction of the science data, a sky frame was used instead of a dark frame as it gives a much better dark measurement, since it was acquired concurrently with the science data. The sky frame also removes any constant additions to the science data due to bias levels. The NISKY task was used to create the sky frame by median combining each individual science image after masking the objects in each image. The NIREDUCE task was used to subtract the sky frame from the individual science images. A flat field image was created by subtracting the median combined “lamps off” / low twilight flat image from each individual “lamps on” / high twilight flat images and then median combing the resultant images. This flat field image was divided by its mean pixel value to create a normalised flat field image. The NIFLAT and NIREDUCE tasks were used to create this normalised flat field image and to divide the individual science images by the normalised flat field image, respectively. For each individual science image, a sky background image was created by median combining the previous and subsequent 5 and 4 science images for the *NIRI* and the *FLAMINGOS* data, respectively, after masking the objects

**Table 2.** Details of the observations of the 23 equatorial and northern hemisphere white dwarfs in the DODO survey

White Dwarf Number	Date Observed	ET [m]	FWHM [']	TW	
0115 + 159	2003-08-17	20	0.65	GN+N	
	2004-08-25	55	0.73	GN+N	
0148 + 467	2003-08-09	54	0.57	GN+N	2
	2005-08-28	75	0.48	GN+N	
0208 + 396	2004-08-25	55	0.57	GN+N	
	2005-08-29	75	0.66	GN+N	
0341 + 182	2004-12-21	55	0.62	GN+N	
	2005-09-04	74	0.58	GN+N	
0435 – 088	2004-12-24	39	0.55	GN+N	
	2005-11-13	75	0.58	GN+N	
0644 + 375	2003-11-03	52	0.59	GN+N	1
	2004-11-02	54	0.65	GN+N	
0738 – 172	2004-12-24	53	0.56	GN+N	
	2005-11-13	75	0.71	GN+N	
0912 + 536	2003-03-22	54	0.63	GN+N	1
	2004-02-09	37	0.64	GN+N	
	2005-01-28	27	0.56	GN+N	
1055 – 072	2004-12-24	49	0.58	GN+N	
	2005-11-16	63	0.77	GN+N	
1121 + 216	2003-03-24	54	0.63	GN+N	1
	2004-02-04	52	0.77	GN+N	2
	2005-01-20	19	0.48	GN+N	1
1134 + 300	2003-03-22	40	0.73	GN+N	1
	2005-02-21	52	0.66	GN+N	
1344 + 106	2003-03-22	54	0.62	GN+N	1
	2004-02-03	54	0.68	GN+N	2
1609 + 135	2003-06-10	53	0.44	GN+N	1
	2004-02-11	51	0.53	GN+N	2
1626 + 368	2003-06-10	46	0.43	GN+N	1
	2004-04-01	47	0.50	GN+N	
1633 + 433	2003-06-09	53	0.61	GN+N	1
	2004-04-01	54	0.52	GN+N	3
1647 + 591	2003-05-17	54	0.58	GN+N	
	2004-02-12	40	0.57	GN+N	
	2005-02-20	54	0.81	GN+N	
1900 + 705	2003-05-17	54	0.58	GN+N	2
	2004-04-06	54	0.54	GN+N	
1953 – 011	2002-06-23	127.5	0.53	GS+F	
	2003-08-10	51	0.52	GN+N	2
2007 – 219	2002-06-21	136.5	0.47	GS+F	
	2003-08-15	53	0.53	GN+N	
	2008-05-20	78	0.53	GN+N	
2047 + 372	2002-06-16	51	0.53	GN+N	
	2003-08-10	54	0.51	GN+N	2
	2004-06-06	54	0.64	GN+N	
2140 + 207	2003-08-11	52	0.53	GN+N	2
	2004-06-07	47	0.80	GN+N	
2246 + 223	2003-08-09	57	0.43	GN+N	2
	2004-06-07	53	0.70	GN+N	
2326 + 049	2002-06-23	148	0.58	GS+F	
	2003-08-09	54	0.49	GN+N	2

Columns: ET is the total exposure time, measured in minutes; FWHM is the full-width at half-maximum, calculated as the average FWHM of stars in the field using SExtractor, measured in arc seconds; TW is the telescope and instrument the data were taken with; GN+N indicates Gemini North and *NIRI* were used; GS+F indicates Gemini South and *FLAMINGOS* were used; Notes: (1) Moderate 60Hz signal, (2) Severe 60Hz signal, (3) Streak across the image due to a bright source just outside the field of view.

in each image. The `XMOSAIC` task in the `XDIMSUM` package was used to create and subtract each sky background image from each individual science image and then create an average combined final stacked image. This task also corrected the bad pixels in each sky subtracted image by using a mask created by the `NIFLAT` task and linearly interpolating across bad columns in each image line. In addition, cosmic ray events are removed by replacing the value of the pixels, which are more than  $5\sigma$  above the median of the pixel values in a surrounding box of  $5 \times 5$  pixels and that are not part of an object, with the local median value.

Saturated pixels (e.g., from the cores of bright stars) can lead to persistence effects in subsequent frames as residual charge remains in the pixels after the array has been reset. Persistence manifests itself as an apparent faint object at the location of the saturated object in the previous image. This faint object can remain for several frames depending on the level of saturation. For the `ALADDIN-II NIRI` array, a highly saturated star will leave a faint object at the level of  $\sim 1\%$  in the subsequent exposure and  $\sim 0.2\%$  in the next one (Hodapp et al. 2003). Persistence affects  $\sim 42\%$  of the science data in Table 2. To remove these persistence effects from the sky background image and from the final stacked image, a mask consisting of the cores of the bright stars in the field from the previous three science images was created for each individual science image and added to the object mask used in the `XMOSAIC` task.

Intermittent pattern noise substantially degraded a large amount of the `NIRI` data throughout 2003 and has also affected some of the data from 2004 and 2005. A diagonal herringbone pattern due to 60 Hz interference (Hodapp et al. 2003) is seen in  $\sim 37\%$  of the `NIRI` data (Table 2). This pattern is reflected symmetrically in each quadrant, due to the fact that the readout of the quadrants, from each corner of the array to the centre of the array along each row, is symmetrical. This pattern is not present in the lab and has been eliminated at times on the telescope, indicating that it arises from the telescope environment and not from the `NIRI` electronics. It was not possible to remove this noise from the `NIRI` data.

Another form of intermittent pattern noise found in the `NIRI` data is due to 50 Hz interference, which creates a horizontal pattern. The constant variations in the rows and columns of each image due to this pattern were removed by collapsing each quadrant along rows and columns and then subtracting the median value from each row and each column separately for each of the quadrants.

Another form of intermittent pattern noise found in the `NIRI` data, which manifests itself as a combined quadrant pattern plus a vertical pattern, was also removed in the same manner. The quadrant pattern occurs due to mismatched bias levels between the quadrants and the vertical pattern has a periodicity of 8 pixels, which corresponds to the 8 amplifier channels reading out each quadrant.

## 5 DATA ANALYSIS

The cleaned final stacked images created using `XMOSAIC` were astrometrically calibrated to within  $\sim 1 - 2''$  using Two Micron All Sky Survey (2MASS; Skrutskie et al. 2006) objects in the field of each white dwarf. The `IRAF` tasks

`CCFIND` and `CCMAP` in the `IMAGES` package were used to calculate the transformation required to match the positions of the objects in the final stacked image with the positions of the objects in the 2MASS catalogue. Objects near the edge of the final stacked image were removed from the transformation calculations. The `CCSETWCS` task was then used to apply this transformation to the final stacked image. The astrometrically calibrated final stacked images were then photometrically calibrated using aperture photometry. Objects in the final stacked image, with instrumental magnitudes  $m_i$ , were matched with objects in the 2MASS catalogue. The instrumental magnitude of the matched object could then be associated with their apparent magnitudes,  $m$ , using the linear formula  $m = m_i + zp$ . The zeropoint,  $zp$ , is therefore equal to the y intercept of the line of best fit to the points in the plot of  $m_i$  against  $m$ . Only photometric 2MASS stars, with a *J* band photometric quality flag equal to “A” (given to objects with a SNR  $> 10$  and a photometric uncertainty,  $\sigma < 0.109$ ), were used to determine the  $zp$ . In addition, objects near the edge of the final stacked image or that were saturated were excluded from this step.

### 5.1 Point Source Detection

The `SExtractor` program (Bertin & Arnouts 1996) was used to detect all objects in the final stacked images with a signal to noise ratio (SNR)  $> 3$ . `SExtractor` determines the position of the centre of an object by computing the first order moments of the isophotal profile of the object, which is adequate for detecting point sources in all the final stacked images in the DODO survey. A “weight map”, created by the `XMOSAIC` task, was used to normalise the noise over the final stacked image. This avoided the detection of spurious sources around the edges of the final stacked image, where only a few of the individual science images contribute. The first pass of `SExtractor` used apertures with diameters ranging from 1 to 20 pixels to determine the aperture size that delivered the highest SNR. Only objects with an internal flag equal to 0, indicating that no problems were found with the detection, were used in the determination of the optimum aperture size. In addition, the ellipticity of the objects, given as  $1 - B/A$ , where  $A$  and  $B$  are the semi-major and semi-minor axes of the object, respectively, was chosen to be  $< 0.2$ . This excluded objects with high ellipticities, such as background galaxies, from the determination of the optimum aperture size. Also, only those objects within the central region of the final stacked image that have a full-width at half-maximum (FWHM)  $< 1''$  were used. This further assisted in removing extended objects. The resulting ideal aperture size was then used to detect all objects in the final stacked images.

### 5.2 Measurement of Proper Motions

The motion of the objects in the field of each white dwarf between the first epoch and second (or third) epoch images was calculated. Since the white dwarf is rarely positioned on the same pixels in each epoch, spurious distortion effects can be seen, which are caused by optical aberrations. As a result, the motion of objects between the two epoch images

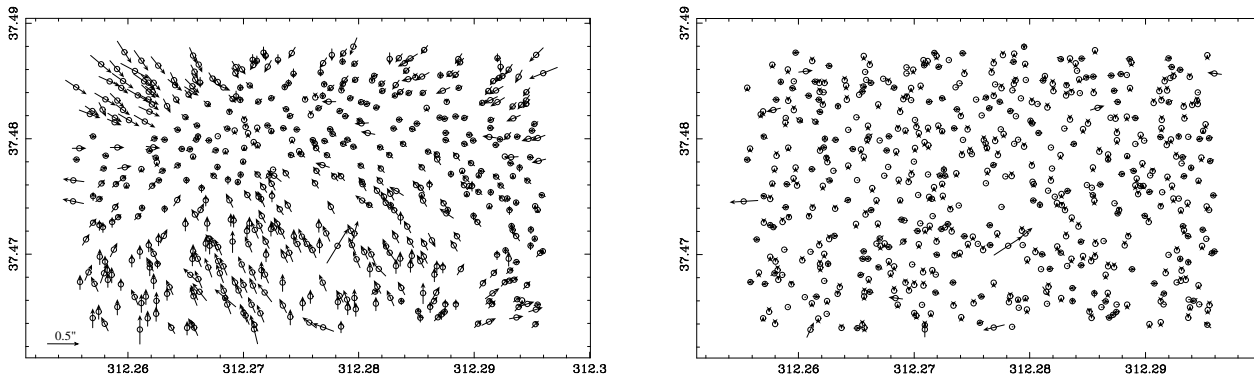


**Figure 1.** Distortion effects before (left) and after (right) the distortion correction was applied to the images of WD 2047 + 372. The x- and y-axes are the R.A. and Dec, respectively, measured in degrees. The arrows in the image indicate the direction and magnitude, multiplied by 20, of the motion of each object in the field between the first epoch and second epoch images.

is seen to be a function of field position (Figure 1). When a large number of background reference stars are present, the two epoch images can be well matched and the distortions can be effectively removed. However, as the number of background reference stars decreases, the two epoch images can not be accurately matched and this is often the limiting factor for astrometric accuracy. The GEOMAP and GEOXYTRAN tasks in the IMAGES package were used to correct for these distortion effects. Objects from the first epoch image were matched to the closest object present in the second (or third) epoch image only if 1) their magnitudes are within 1 mag, 2) the SExtractor internal flag  $\leq 3$ , which indicates a good detection, 3) the ellipticity of the object is  $< 0.5$ . This excluded objects with very high ellipticities, such as background galaxies, from the matching procedure. In some cases, the closest object was too far away to be a true match, so a clipping factor was introduced to remove these mismatches.

### 5.3 Limits and Errors

The completeness limit for each final stacked image was estimated by determining the magnitude at which 90% and 50% of inserted artificial stars were recovered from each image. The STARLIST task was used to create a list of 200 randomly positioned artificial stars at a magnitude of  $J = 19.0$  mag. The MKOBJECTS task was used to insert the artificial stars into the final stacked image. SExtractor was then used to detect all objects in the image, including the artificial stars. The calculated magnitudes of the artificial stars were checked to ensure they were equal to  $J = 19.0$  mag. Using the same artificial star list, the MKOBJECTS and SExtractor steps were repeated for magnitudes between  $19.1 \leq J \leq 24.0$  mag in 0.1 magnitude steps. The entire process was then repeated a further 50 times, equivalent to a total of 10,000 inserted artificial stars for each 0.1 magnitude bin. Plots of the percentage of artificial stars recovered against the apparent  $J$  magnitudes of the artificial stars were created. The number of artificial stars recovered

was often much less than 100% at the brighter  $J$  magnitudes as some stars were lost within the point spread function (PSF) of other real objects or artificial stars. The motion of an object can be calculated only when the object is detected in both epochs. Assuming that the probability of detecting an object in the first epoch image,  $P_1$ , is independent from the probability of detecting an object in the second epoch image,  $P_2$ , the probability of detecting an object in both epochs is  $P_1 \times P_2$ . Therefore, by multiplying the individual completeness limits for each epoch, a combined completeness limit for both epoch images can be determined. This assumption is valid for objects near the completeness limit. However, it is not valid for the bright objects not detected due to the fact that they are within the PSF of other real objects or artificial stars. Therefore, the completeness limits at the brighter  $J$  magnitudes are underestimated.

The “COND” evolutionary models for cool brown dwarfs and extrasolar planets (Baraffe et al. 2003), along with the magnitudes at which 90% and 50% of artificial stars were recovered, were used to estimate the minimum mass of a companion which could be detected in both epoch images. The models predict the absolute magnitudes of substellar objects depending upon their age. Isabelle Baraffe kindly supplied these models for the total ages determined for all the white dwarfs in the DODO survey. The total age is equal to the sum of the main sequence progenitor lifetime and white dwarf cooling age, both of which depend upon evolutionary models. While the cooling age errors are small and well constrained (Fontaine et al. 2001), and the scatter in the empirical IFMR is significantly reducing as more and higher quality observations are made of white dwarfs in open clusters (Casewell et al. 2008), the main sequence progenitor lifetimes rely on models which are difficult to calibrate (e.g., Catalán et al. 2008). Therefore, to take these uncertainties into account, a conservative error of  $\pm 25\%$  is applied to the total age of each white dwarf (note that the white dwarf cooling age is the dominant timescale for most of the targets in the DODO survey, as shown in Table 1). However, at ages  $> 1$  Gyr, the “COND” evolutionary models indi-

cate that the absolute magnitudes of substellar objects are relatively insensitive to changes in their age, implying that even with a  $\pm 25\%$  error, the resulting error on the mass of a companion is small (Table 3).

The detection of a companion with a mass equal to the minimum mass determined using the completeness limit will only be possible if the companion is outside the extent of the PSF of the white dwarf. In addition, it is expected that the orbital radius of any companions that avoid direct contact with the red giant envelope will expand, which would increase the projected physical separation between the companion and the white dwarf. The majority of the DODO survey observations were acquired in good seeing conditions, so the minimum projected physical separation at which a companion could be found around each white dwarf was taken to be  $3''$ . Beyond this distance, the contribution of the flux from the white dwarf was assumed to be minimal. A more careful treatment of the PSF of the white dwarf could allow companions to be uncovered within  $3''$  and will be dealt with in a future publication. The maximum projected physical separation at which a companion could be found around each white dwarf is limited by the field of view covered by both epochs. The completeness limit is only valid in the central region of each final stacked image, where all the individual images contribute. The useable field of view decreases further when the two epoch images are matched as the white dwarf is rarely positioned on the same pixels in each epoch image. The minimum and maximum projected physical separations at which a companion could be found around the main sequence progenitor can also be estimated, since the orbital radius of any companions around the main sequence progenitor will expand by a factor of  $M_{\text{MS}}/M_{\text{WD}}$  during stellar evolution.

## 6 RESULTS

Figures 2 – 24 show the results for each of the 23 equatorial and northern hemisphere white dwarfs from the DODO survey. Using the combined completeness limit for each white dwarf, an estimate of the minimum mass of a companion which could be detected in both epoch images is calculated. The range of projected physical separations at which a companion of this mass could be found around each white dwarf and the corresponding range of projected physical separations around the main sequence progenitors is determined. These results are summarised in Table 3. Comments are made only on interesting objects.

### 6.1 WD 0644 + 375

The mass of WD 0644 + 375 used throughout this paper was determined by assuming that the core of this white dwarf is made partly of strange matter (Mathews et al. 2006). This unusual core composition was suggested as a way to explain the inconsistency between the radius determined from the parallax of WD 0644 + 375, obtained from Hipparcos data, and the radius predicted using a mass–radius relation, which assumes the core of the white dwarf is composed primarily of carbon (Provencal et al. 1998). The mass of the white dwarf was originally determined by Bergeron et al. (1992) to be  $0.66 M_{\odot}$ , but this predicted a radius that

was significantly larger than predicted using the parallax. Therefore, the slightly lower mass of  $0.54 M_{\odot}$  determined by Fontaine et al. (2007) is used here to determine the total age of the white dwarf, since this mass provides a radius consistent with observations. Note that a companion with a mass of  $5 \pm 1 M_{\text{Jup}}$  could have been detected if the larger white dwarf mass was used to determine the total age of the white dwarf.

### 6.2 WD 0738 – 172

WD 0738 – 172 is a member of a known common proper motion binary. The secondary star of this binary system is an M6 main sequence star (Monteiro et al. 2006) with an orbital radius of  $\sim 262$  AU (Poveda et al. 1994). The main sequence secondary does not appear in the proper motion diagram as it was saturated in the 2005 second epoch image, making it unavailable for proper motion measurements. The overall decrease in the completeness limit, compared to the other white dwarfs, of the images acquired of WD 0738 – 172 is due to the higher proportion of artificial stars inserted within the PSF of the bright secondary.

### 6.3 WD 1626 + 368

Recent MIR observations of the helium atmosphere DZ white dwarf WD 1626 + 368 show no evidence of a dust disk (Mullally et al. 2007). However, the abundance of carbon relative to iron in the atmosphere of WD 1626 + 368 is 10 times below the solar abundance, similar to the carbon deficient asteroids in the Solar System. Therefore, external pollution from such asteroids naturally explains the abundances of the metals in the atmosphere of this white dwarf (Jura 2006). The possible presence of asteroids in orbit around WD 1626 + 368 represents an increased probability of the existence of an old planetary system. However, the motion of this white dwarf between the first epoch and second epoch images is large enough to confidently state that there are no common proper motion companions to WD 1626 + 368 within the limits given in Table 3.

### 6.4 WD 1633 + 433

Although no dust disk has been found in orbit around the DAZ white dwarf WD 1633 + 433, the presence of metals in its atmosphere may indicate the existence of an old planetary system. The 2003 first epoch image of WD 1633 + 433 was degraded by 60 Hz interference (Table 2), which has decreased the completeness limit of this image. In addition, the 2004 second epoch image of WD 1633 + 433 was degraded by a large streak across the image, due to a source just outside the field of view. However, this streak is not present in the first epoch image. It is likely that these effects have introduced the large scatter in the motions of objects with magnitudes  $J > 21$  mag between the 2003 first epoch and 2004 second epoch images (Figure 25), particularly in the region of the streak. This suggests that the error on the motion of these faint objects is comparable to the motion of WD 1633 + 433 (Table 1). As a result, multiple objects appear to have motions similar to the motion of the white dwarf (the two objects with motions closest to the motion of



WD 1633 + 433 lie on the streak). Real common proper motion companions to WD 1633 + 433 cannot be distinguished from non-moving background objects. Therefore, a third

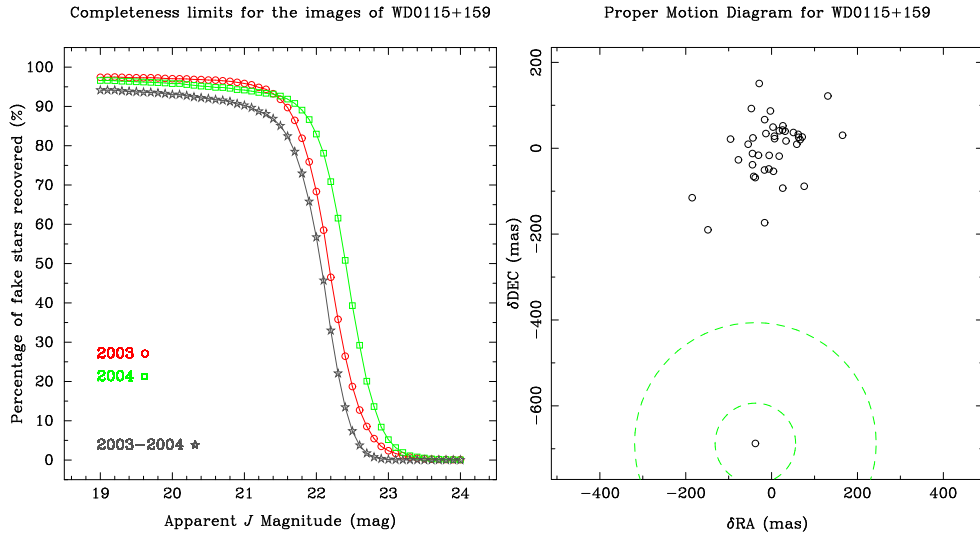


**Figure 2.** The completeness limit (left) shows the percentage of artificial stars recovered by SExtractor from the 2003 first epoch and 2004 second epoch images acquired of WD 0115 + 159, against the apparent  $J$  magnitude of the artificial stars. The proper motion diagram (right) shows the motion of all objects in the field of WD 0115 + 159 between the first epoch and second epoch images. The dashed green circles represent the  $1\sigma$  and  $3\sigma$  scatter of the distribution of the motions of all objects excluding the white dwarf, centred on the white dwarf, to help determine possible common proper motion companions to the white dwarf.

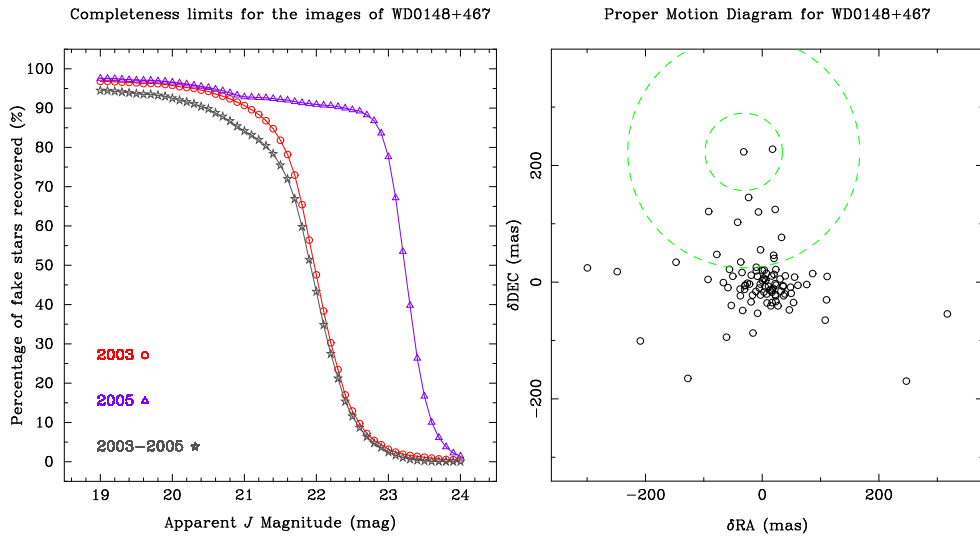


**Figure 3.** The completeness limit (left) and the proper motion diagram (right) for WD 0148 + 467.

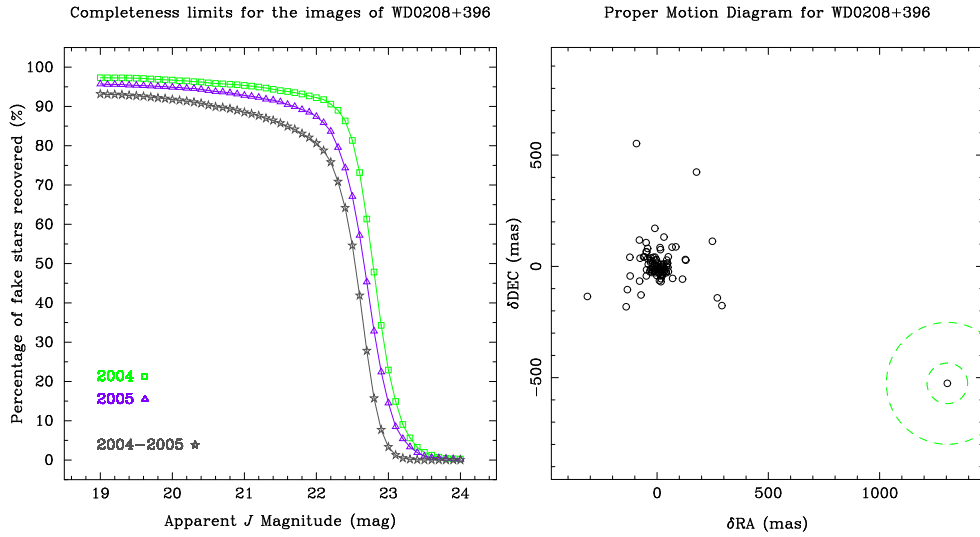


Figure 4. The completeness limit (left) and the proper motion diagram (right) for WD 0208 + 396.

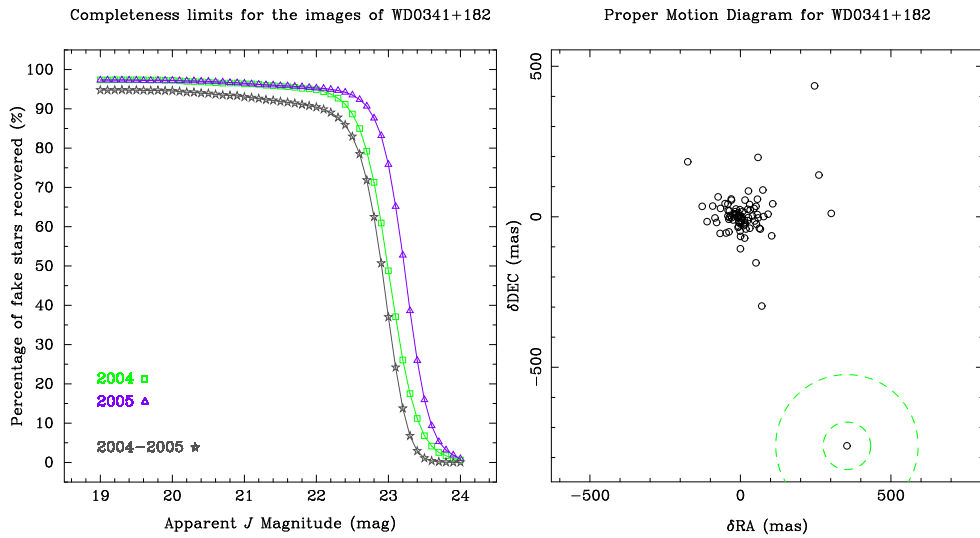


Figure 5. The completeness limit (left) and the proper motion diagram (right) for WD 0341 + 182.

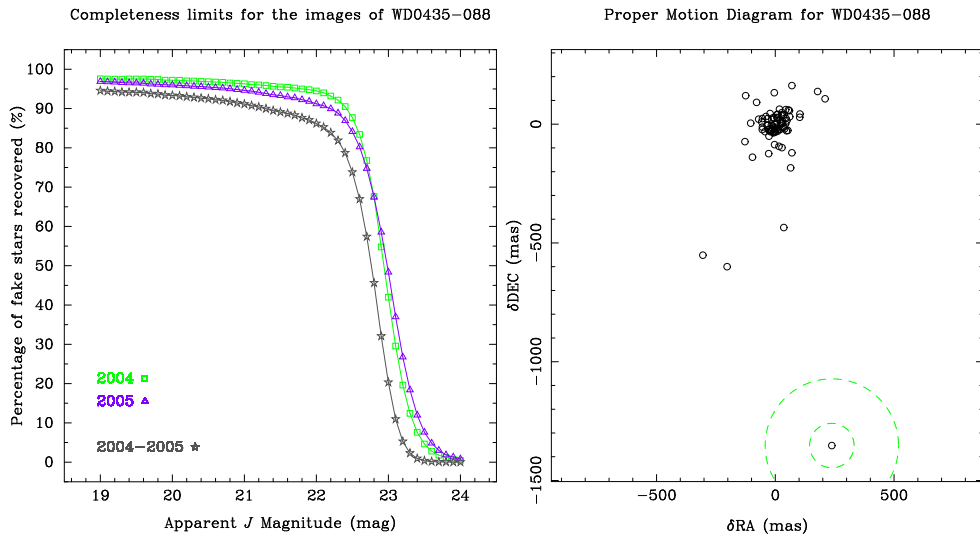


Figure 6. The completeness limit (left) and the proper motion diagram (right) for WD 0435 - 088.

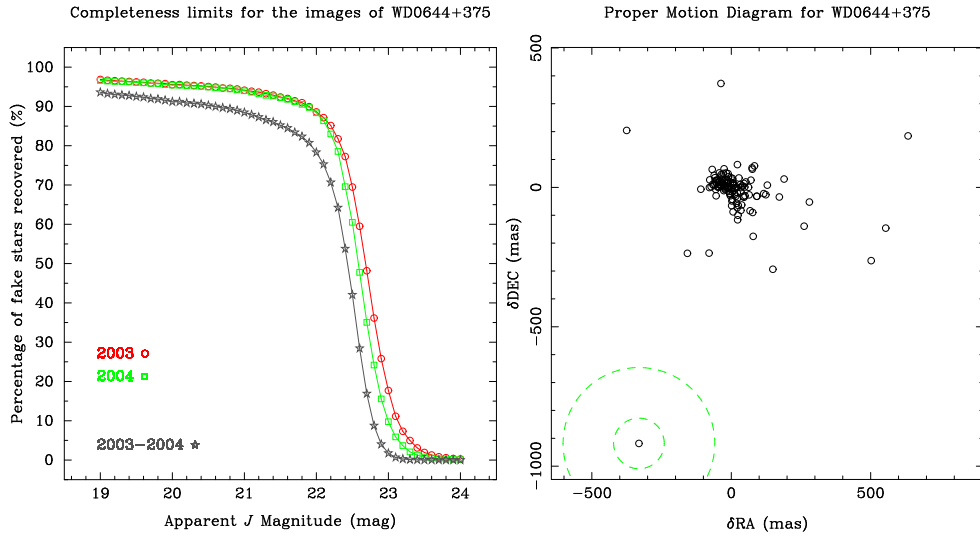


Figure 7. The completeness limit (left) and the proper motion diagram (right) for WD 0644 + 375.

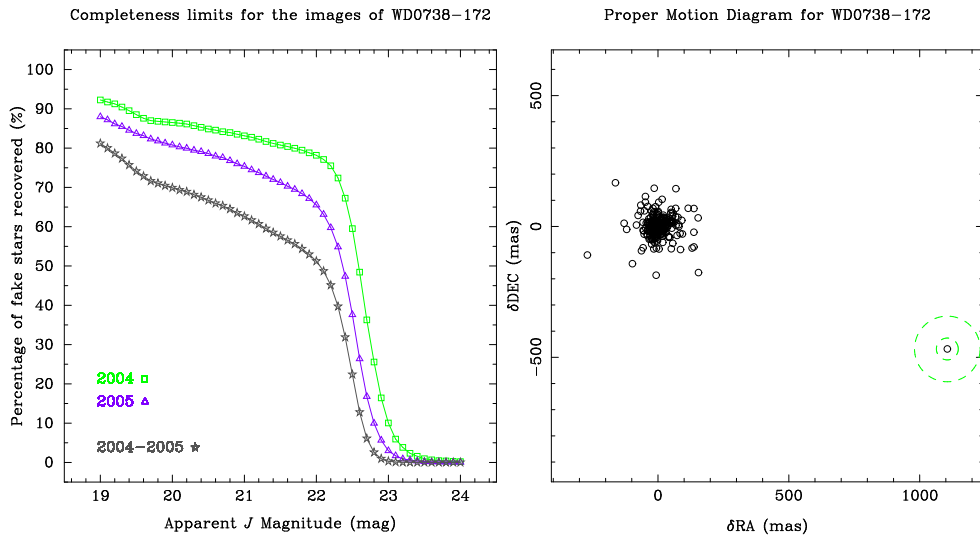


Figure 8. The completeness limit (left) and the proper motion diagram (right) for WD 0738 - 172.

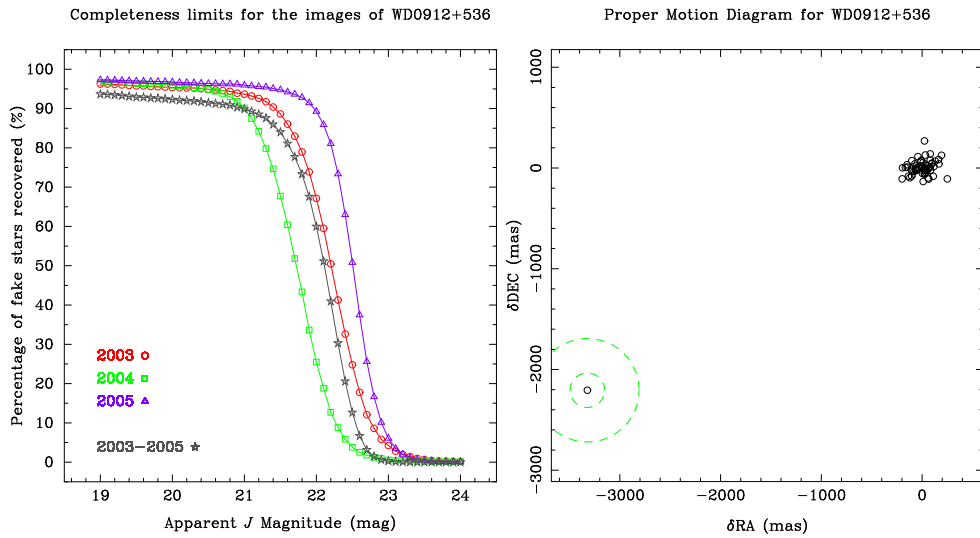


Figure 9. The completeness limit (left) and the proper motion diagram (right) for WD 0912 + 536.

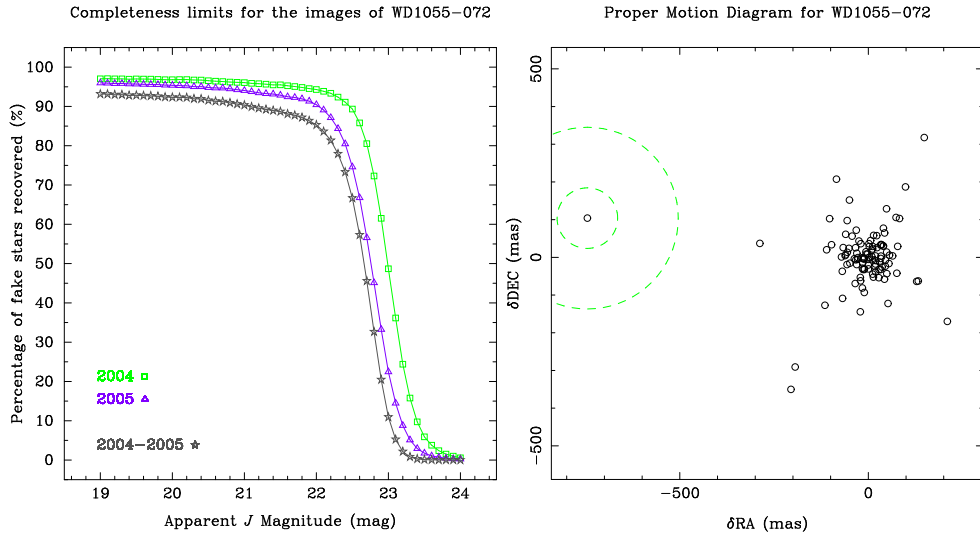


Figure 10. The completeness limit (left) and the proper motion diagram (right) for WD 1055 – 072.

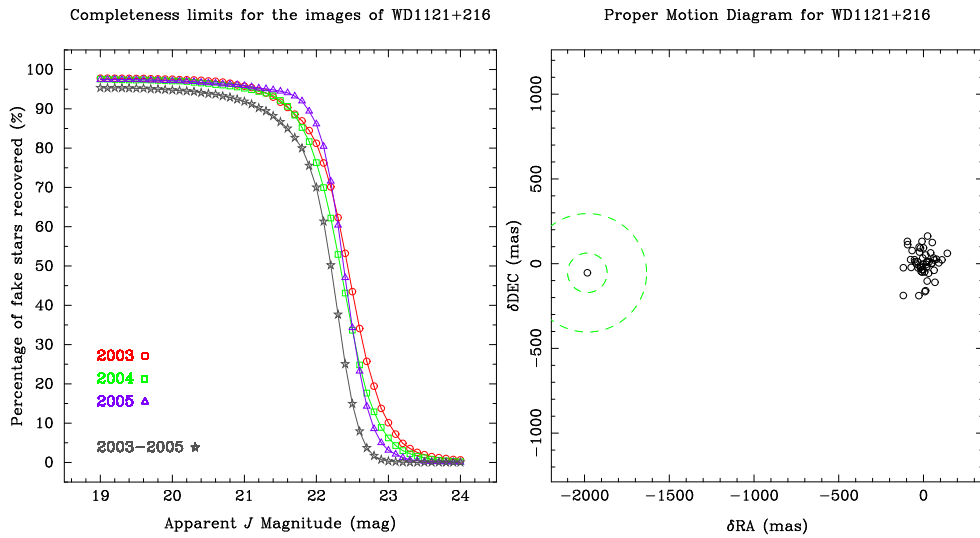


Figure 11. The completeness limit (left) and the proper motion diagram (right) for WD 1121 + 216.

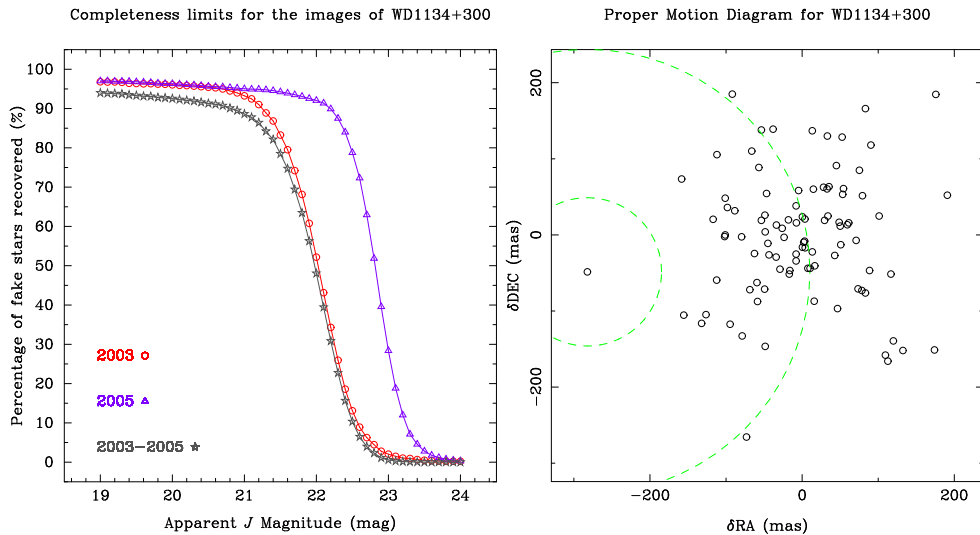
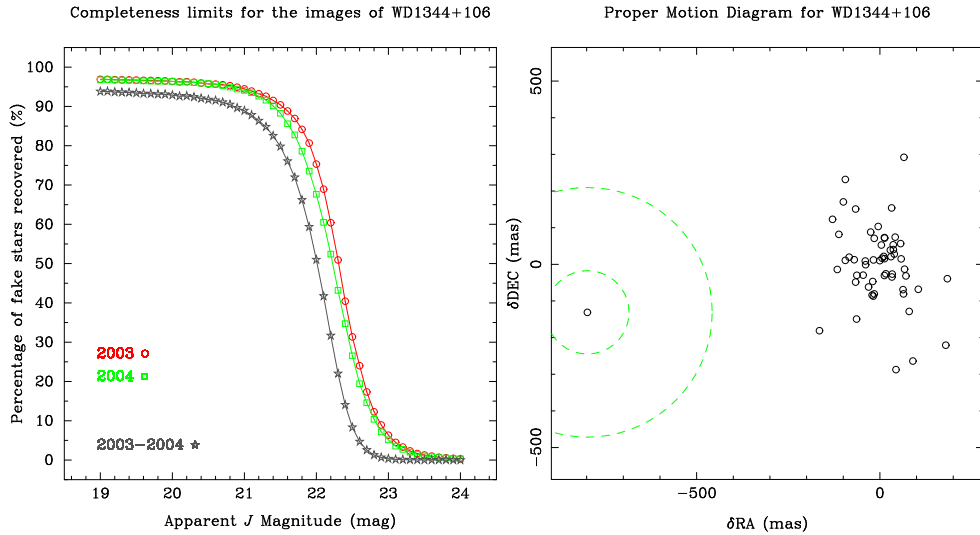
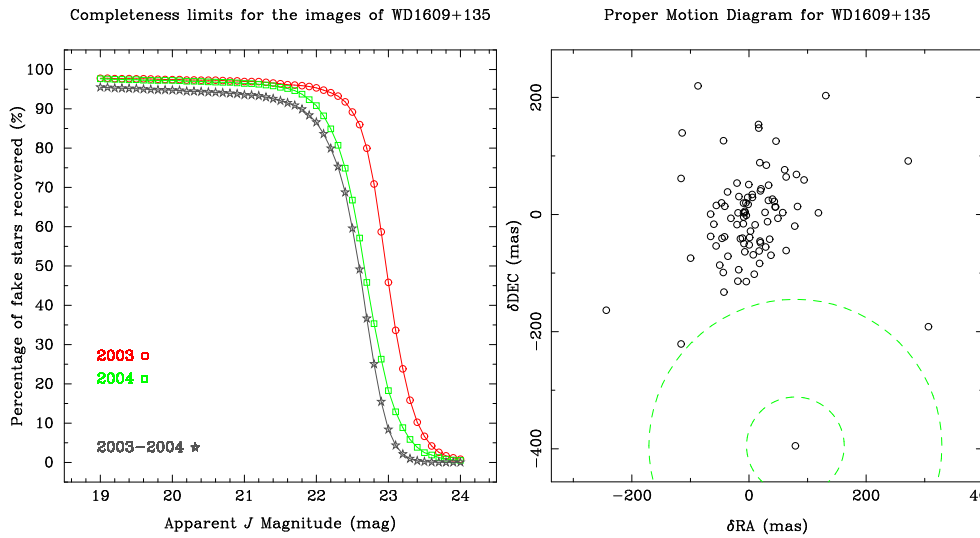


Figure 12. The completeness limit (left) and the proper motion diagram (right) for WD 1134 + 300.



**Figure 13.** The completeness limit (left) and the proper motion diagram (right) for WD 1344 + 106.



**Figure 14.** The completeness limit (left) and the proper motion diagram (right) for WD 1609 + 135.

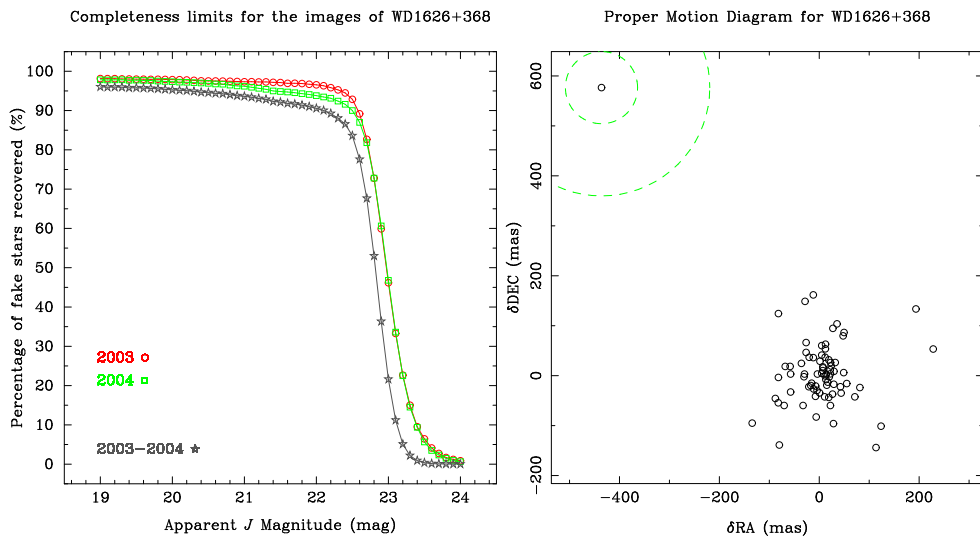


**Figure 15.** The completeness limit (left) and the proper motion diagram (right) for WD 1626 + 368.

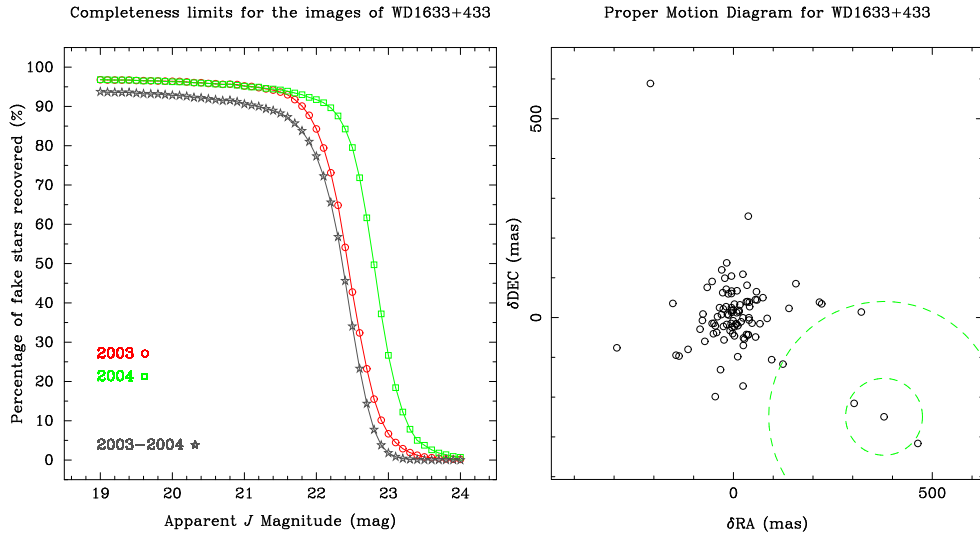


Figure 16. The completeness limit (left) and the proper motion diagram (right) for WD 1633 + 433.

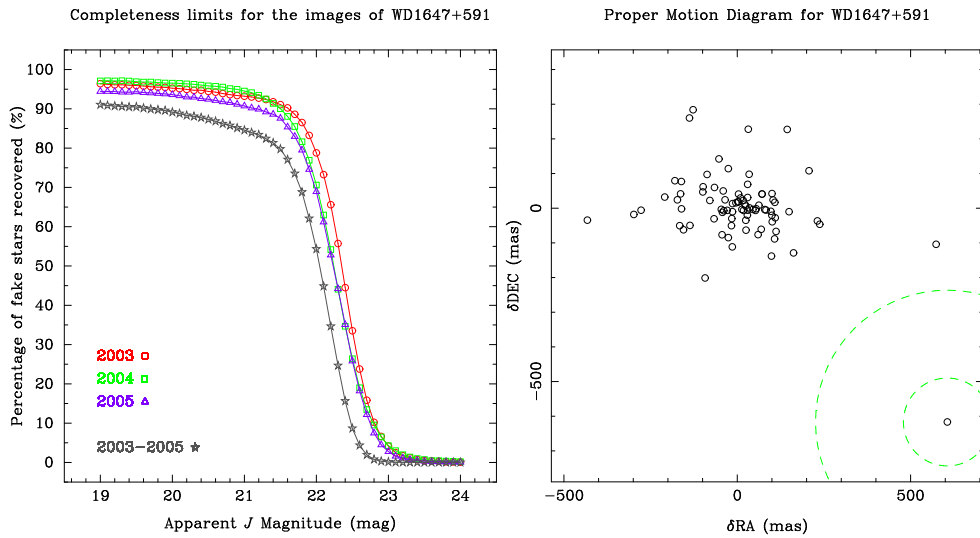


Figure 17. The completeness limit (left) and the proper motion diagram (right) for WD 1647 + 591.

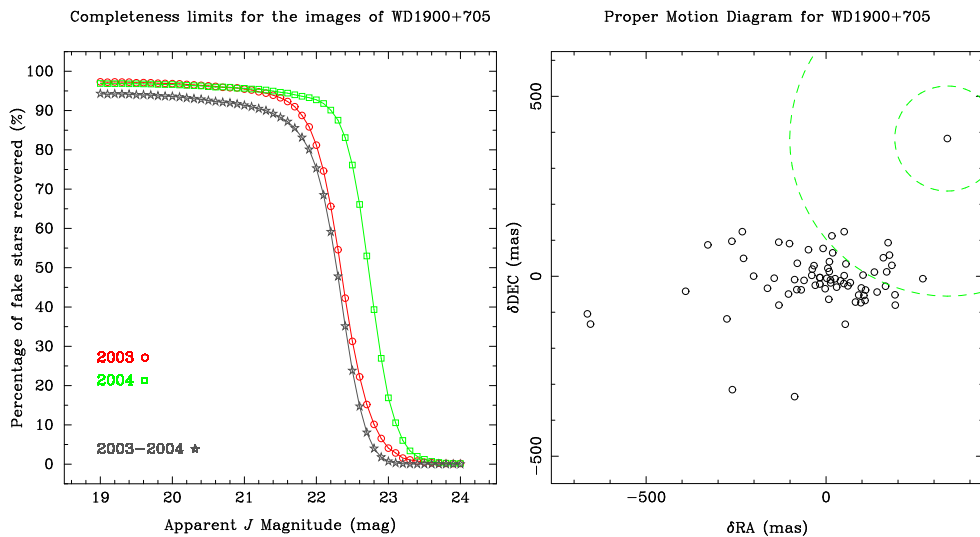


Figure 18. The completeness limit (left) and the proper motion diagram (right) for WD 1900 + 705.

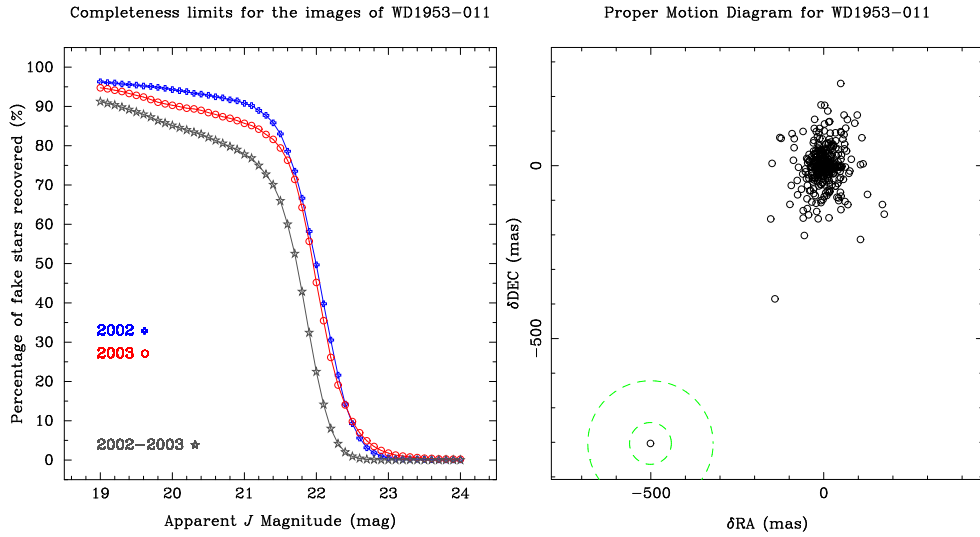


Figure 19. The completeness limit (left) and the proper motion diagram (right) for WD 1953 – 011.

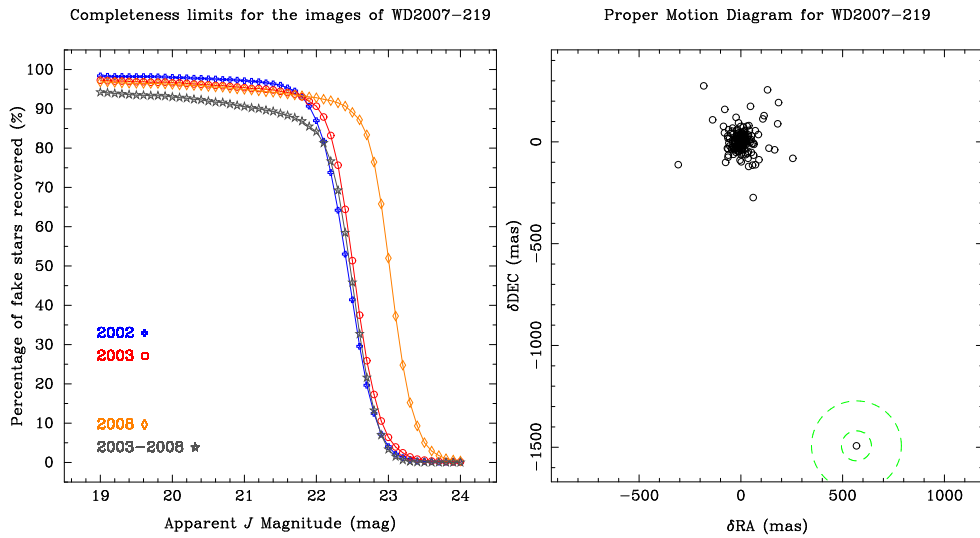


Figure 20. The completeness limit (left) and the proper motion diagram (right) for WD 2007 – 219.

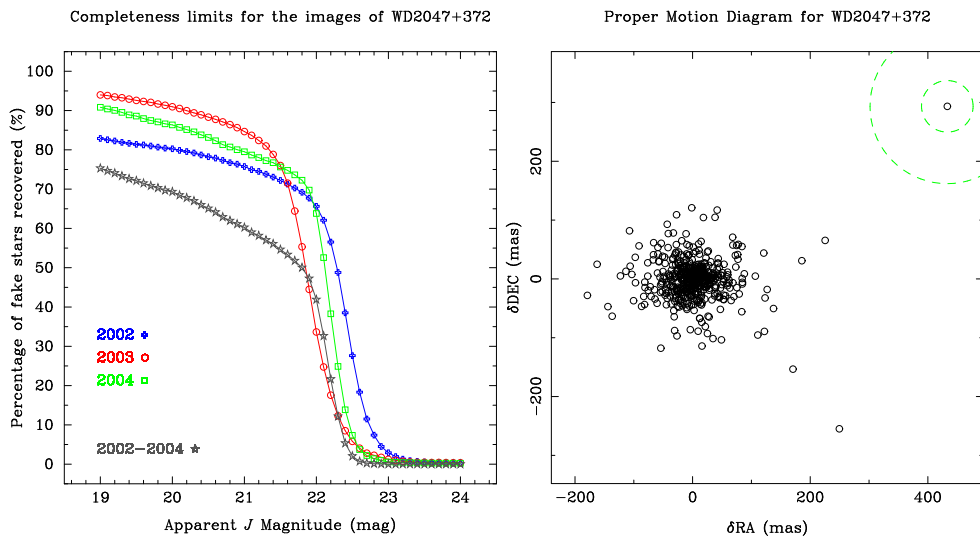


Figure 21. The completeness limit (left) and the proper motion diagram (right) for WD 2047 + 372.



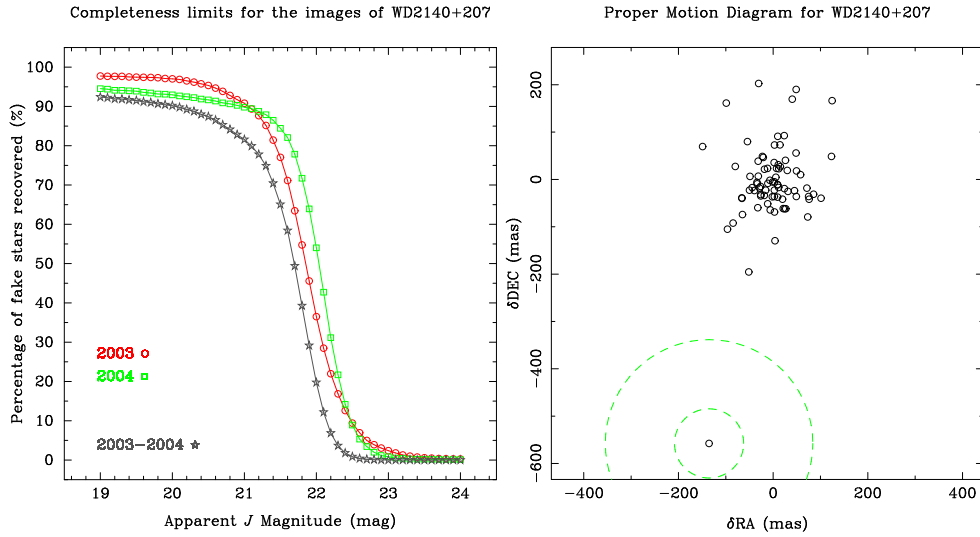


Figure 22. The completeness limit (left) and the proper motion diagram (right) for WD 2140 + 207.

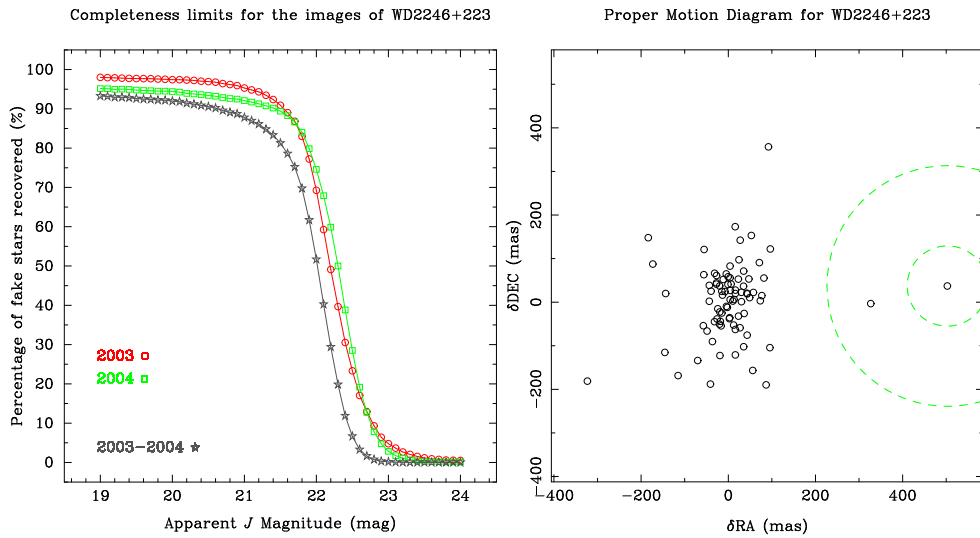


Figure 23. The completeness limit (left) and the proper motion diagram (right) for WD 2246 + 223.

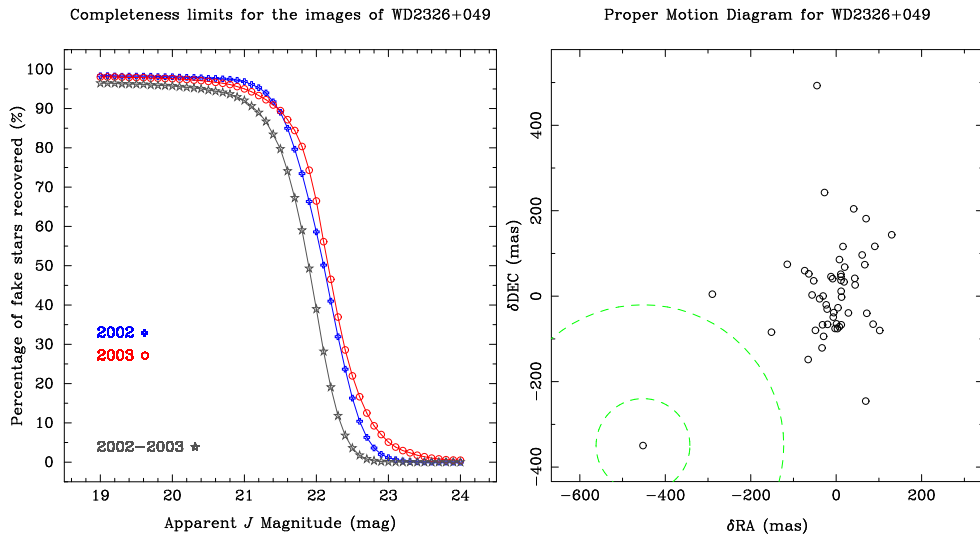


Figure 24. The completeness limit (left) and the proper motion diagram (right) for WD 2326 + 049.

epoch image is required to determine if any of these objects are genuine common proper motion companions.

### 6.5 WD 2007 – 219

A single object with a magnitude of  $J \sim 22$  mag appeared to have a motion similar to that of WD 2007 – 219 between the 2002 first epoch image and 2003 second epoch images (Figure 26). This candidate companion was detected with a SNR of  $\sim 9$  and  $\sim 11$  in the first epoch and second epoch images, respectively. The magnitude of the motion of the candidate was  $\sim 440$  mas. In comparison, the rms of the magnitude of the motion of all point sources in the field with  $21.5 < J < 22.5$  mag is  $\sim 130$  mas. The motion of the candidate was  $> 3$  times larger than this mean error and was clearly separated from the other faint objects in the field. Therefore, both the magnitude and direction of its motion was entirely consistent with that of the white dwarf, suggesting that the candidate was a true common proper motion companion. The candidate would have a mass of  $7 \pm 1 M_{\text{Jup}}$  and a projected physical separation of  $\sim 980$  AU if it were confirmed to be a common proper motion companion to WD 2007 – 219. A third epoch image was recently acquired to investigate whether this apparently co-moving candidate was real. Unfortunately, the new observation showed that this object is in fact a non-moving background object. The *NIRI* 2008 third epoch image is less noisy than the *NIRI* 2003 second epoch image, which has improved the completeness limit and shows the candidate to have some structure. Therefore, it is likely to be a galaxy. In summary, these observations could have detected a companion with a mass of  $7 \pm 1 M_{\text{Jup}}$ , corresponding to an effective temperature of  $\sim 370$  K (Baraffe et al. 2003), between a projected physical separation of 55 – 831 AU with a 50% probability (Table 3). The motion of this white dwarf between the first epoch and third epoch images is large enough to confidently state that there are no common proper motion companions to WD 2007 – 219 within these limits.

### 6.6 WD 2140 + 207

The mass of this DQ white dwarf used throughout this paper ( $0.49 M_{\odot}$ ) was determined by including effects from the carbon present in its atmosphere (Dufour, Bergeron & Fontaine 2005), while Debes et al. (2006) use a white dwarf mass of  $0.62 M_{\odot}$  (Bergeron, Leggett & Ruiz 2001), which was derived using a pure helium model. In contrast, a companion with a mass of  $9^{+1}_{-2} M_{\text{Jup}}$  could have been detected if the larger white dwarf mass was used to determine the total age of the white dwarf.

### 6.7 WD 0148 + 467, WD 1134 + 300, WD 1900 + 705, WD 2246 + 223

The 2003 first epoch images of WD 0148 + 467, WD 1134 + 300, WD 1900 + 705 and WD 2246 + 223 were degraded by severe 60 Hz interference (Table 2), which significantly decreased the completeness limit of these images. It is likely that this interference has introduced the large scatter in the motions of faint objects between the 2003 first epoch

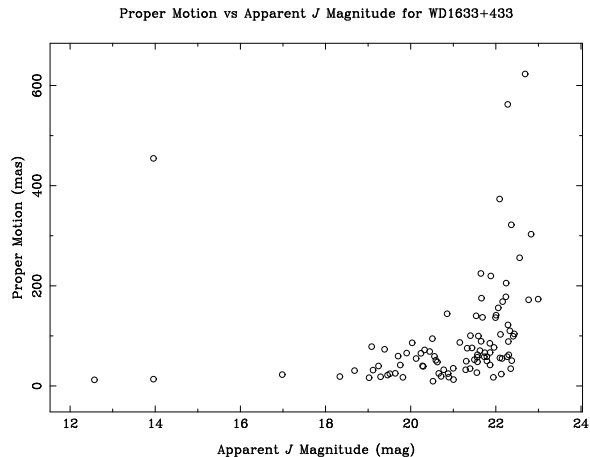


**Figure 25.** The motion of the objects between the first epoch and second epoch images of WD 1633 + 433. The white dwarf has a magnitude of  $J \sim 14$  mag.

and 2004 / 2005 second epoch images (Figures 27, 28, 29 and 30). This suggests that the error on the motion of these faint objects is comparable to the motion of the white dwarfs. As a result, multiple objects appear to have motions similar to the motion of the white dwarfs. In the case of WD 2246 + 223, a single object appears to have a motion similar to the motion of WD 2246 + 223. The candidate common proper motion companion is detected with a SNR of  $\sim 5$  in both epoch images. If the candidate is confirmed to be a common proper motion companion to WD 2246 + 223, it would have a mass of  $9 \pm 1 M_{\text{Jup}}$  and a projected physical separation of  $\sim 840$  AU. This corresponds a projected physical separation of  $\sim 160$  AU around the main sequence progenitor, assuming an expansion factor of  $M_{\text{MS}}/M_{\text{WD}} \sim 5.1 M_{\odot}/0.97 M_{\odot} \sim 5.3$ . However, due to the presence of 60 Hz interference, the measurement of the motion of the candidate between the first epoch and second epoch images may be inaccurate. In addition, there are two other objects which appear to have the same magnitude of motion as the candidate, reducing the probability that the candidate is a genuine common proper motion companion. Therefore, a third epoch image is required, for all four of these white dwarfs, to determine if any of these objects are genuine common proper motion companions.

## 7 DISCUSSION

No common proper motion companions within the limits given in Table 3 were discovered around 18 of the 23 equatorial and northern hemisphere white dwarfs in the DODO survey. Of these, 11 white dwarfs were subject to previous searches for substellar companions (Table 4). The DODO survey extends out to a much larger projected physical separation in each case and places a new lower, upper limit on the mass of any possible companion in orbit around 7 of these white dwarfs (Tables 3 and 4). For the remaining 5 targets, multiple objects in each field of view appear to have motions similar to the motion of the white dwarfs.

**Table 3.** Results for the 23 equatorial and northern hemisphere white dwarfs in the DODO survey

White Dwarf	$t_{\text{tot}}$ [Gyr]	90% $J$ [mag]	90% $M$ [ $M_{\text{Jup}}$ ]	90% $T$ [K]	50% $J$ [mag]	50% $M$ [ $M_{\text{Jup}}$ ]	50% $T$ [K]	WD Orbit [AU]	MS Orbit [AU]	$1\sigma$ error [mas]	
0115 + 159	1.7	21.0	$10^{+2}_{-1}$	430	22.0	$8^{+1}_{-1}$	380	46 - 675	11 - 160	94	
0148 + 467	2.5	20.4	$16^{+5}_{-3}$	480	21.9	$10^{+2}_{-1}$	390	48 - 457	14 - 138	66	1,2
0208 + 396	2.6	20.5	$16^{+5}_{-3}$	480	22.5	$9^{+1}_{-1}$	360	50 - 758	13 - 194	91	
0341 + 182	3.3	22.0	$13^{+3}_{-2}$	400	22.9	$10^{+2}_{-1}$	360	57 - 801	16 - 222	79	
0435 - 088	4.1	21.2	$13^{+3}_{-2}$	380	22.7	$9^{+1}_{-2}$	320	28 - 408	9 - 124	94	
0644 + 375	2.1	20.5	$13^{+3}_{-0}$	460	22.4	$8^{+1}_{-1}$	360	46 - 652	17 - 236	124	1
0738 - 172	2.4	—	—	—	22.0	$7^{+1}_{-1}$	320	27 - 379	7 - 96	42	3
0912 + 536	3.0	20.9	$13^{+0}_{-2}$	410	22.1	$9^{+1}_{-2}$	350	31 - 419	7 - 93	171	1
1055 - 072	3.3	21.0	$13^{+3}_{-2}$	400	22.6	$9^{+1}_{-1}$	340	36 - 503	8 - 103	80	
1121 + 216	2.3	21.2	$10^{+2}_{-1}$	390	22.2	$8^{+2}_{-1}$	350	40 - 605	9 - 134	117	1
1134 + 300	0.37	20.8	$5^{+0}_{-1}$	440	21.9	$3^{+1}_{-0}$	350	46 - 664	9 - 127	97	1,2
1344 + 106	2.5	20.8	$16^{+5}_{-3}$	480	22.0	$13^{+0}_{-2}$	440	60 - 865	14 - 208	114	1
1609 + 135	2.8	21.7	$13^{+3}_{-2}$	420	22.5	$10^{+2}_{-1}$	380	55 - 642	10 - 117	83	1
1626 + 368	2.2	22.1	$9^{+1}_{-1}$	380	22.8	$8^{+1}_{-1}$	360	48 - 535	13 - 141	72	1
1633 + 433	3.0	21.1	$13^{+3}_{-0}$	410	22.3	$10^{+2}_{-2}$	370	45 - 533	10 - 123	97	1,2,4
1647 + 591	0.91	19.6	$9^{+1}_{-1}$	480	22.0	$5^{+0}_{-1}$	350	33 - 372	7 - 77	127	
1900 + 705	1.1	21.2	$7^{+1}_{-1}$	400	22.2	$5^{+1}_{-0}$	330	39 - 452	8 - 89	146	1,2
1953 - 011	2.1	19.2	$16^{+5}_{-0}$	510	21.7	$8^{+1}_{-1}$	360	34 - 509	7 - 111	60	1
2007 - 219	1.4	21.2	$10^{+0}_{-2}$	450	22.4	$7^{+1}_{-1}$	370	55 - 831	12 - 189	74	
2047 + 372	0.89	—	—	—	21.8	$6^{+1}_{-0}$	390	54 - 202	12 - 46	44	1
2140 + 207	4.4	20.0	$21^{+0}_{-0}$	490	21.6	$13^{+3}_{-0}$	370	38 - 542	13 - 181	73	1
2246 + 223	1.7	20.6	$13^{+3}_{-0}$	490	22.0	$9^{+1}_{-1}$	400	57 - 835	11 - 157	92	1,2
2326 + 049	1.1	21.1	$7^{+1}_{-1}$	400	21.8	$6^{+1}_{-1}$	370	41 - 396	9 - 89	110	1,5

Columns:  $t_{\text{tot}}$  is the “COND” evolutionary model age used; 90% and 50% gives the 90% and 50% completeness limits in terms of apparent  $J$  magnitude, mass,  $M$ , measured in Jupiter masses, and effective temperature,  $T$ , measured in Kelvin, respectively; WD Orbit is the range of projected physical separations at which a companion of that mass could be found around the white dwarf, measured in AU; MS Orbit is the range of projected physical separations at which a companion of that mass could be found around the main sequence progenitor, measured in AU;  $1\sigma$  error is the  $1\sigma$  scatter of the distribution of the motions of all objects in the field, excluding the white dwarf, measured in milli arc seconds. Notes: (1) 60Hz signal present in at least one epoch image, (2) A third epoch image is required, (3) A common proper motion companion is known to orbit this white dwarf, (4) Streak across one epoch image due to a bright source just outside the field of view, (5) A dust disk is known to orbit this white dwarf.

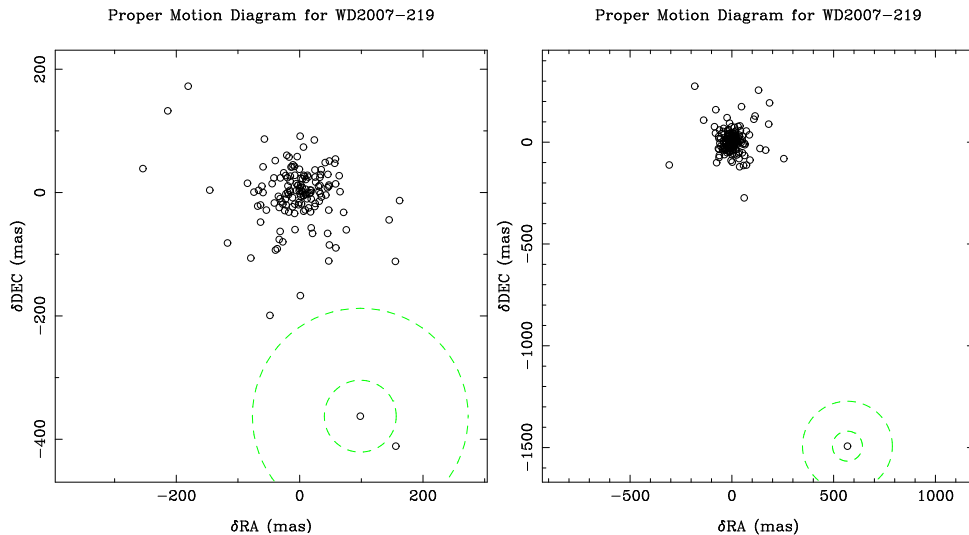


**Figure 26.** The proper motion diagram (left) shows the motion of all objects in the field of WD 2007 - 219 between the first epoch and second epoch images. The dashed green circles represent the  $1\sigma$  and  $3\sigma$  scatter of the distribution of the motions of all objects excluding the white dwarf, centred on the white dwarf, to help determine possible common proper motion companions to the white dwarf. A single object appears to have a motion similar to that of WD 2007 - 219. The latest proper motion diagram (right), utilising the 2008 third epoch image, shows that there are no common proper motion companions to WD 2007 - 219.

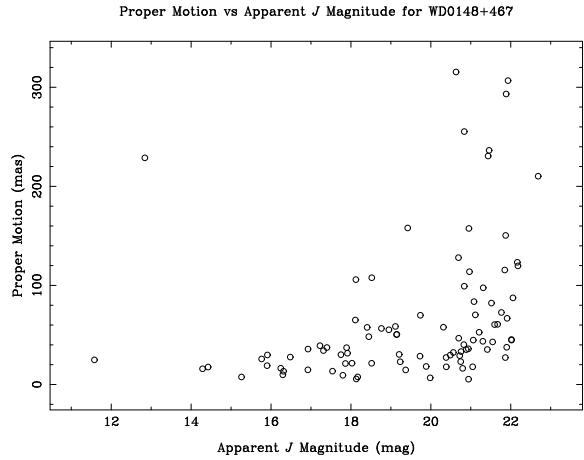
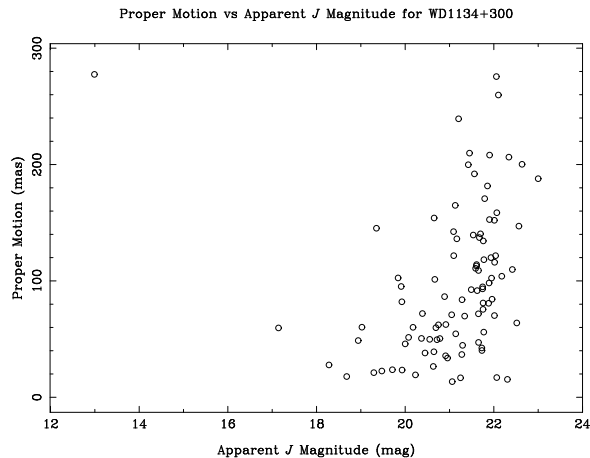
**Table 4.** Previous searches for substellar companions around the 23 equatorial and northern hemisphere white dwarfs in the DODO survey

White Dwarf	$M$ [ $M_{\text{Jup}}$ ]	WD Orbit ["]	WD Orbit [AU]	Ref
0115 + 159	-	-	-	
0148 + 467	-	-	-	
0208 + 396	10	0.9 - 10	15 - 167	1
0341 + 182	-	-	-	
0435 - 088	-	-	-	
0644 + 375	-	-	-	
0738 - 172	-	-	-	
0912 + 536	12	1 - 7	10 - 72	2
1055 - 072	14	1 - 7	12 - 85	2
1121 + 216	11	1 - 7	13 - 94	2
1134 + 300	-	-	-	
1344 + 106	14	Unresolved		3
1609 + 135	-	-	-	
1626 + 368	14	1 - 7	16 - 112	2
1633 + 433	14	1 - 7	15 - 106	2
	14	Unresolved		3
1647 + 591	-	-	-	
1900 + 705	-	-	-	
1953 - 011	10	1 - 7	11 - 80	2
2007 - 219	-	-	-	
2047 + 372	-	-	-	
2140 + 207	10	1 - 7	13 - 88	2
2246 + 223	9	1 - 7	19 - 133	2
2326 + 049	6	1 - 5	14 - 68	4

Columns:  $M$  is the minimum mass of a companion that could be found around the white dwarf, measured in Jupiter masses; WD Orbit is the range of projected physical separations at which a companion of that mass could be found around the white dwarf, measured in arc seconds and determined in AU using the distance to the white dwarf, measured in parsecs, taken from van Altena, Lee & Hoffleit (1995) (Table 1); Two targets were part of a search for companions through the detection of an infrared excess and are denoted by “Unresolved”; Ref = References: (1) Debes, Sigurdsson & Woodgate (2005b), (2) Debes, Ge & Ftaclas (2006), (3) Farihi, Becklin & Zuckerman (2008), (4) Debes, Sigurdsson & Woodgate (2005a).

Two of these stars, WD 0148 + 467 and WD 1134 + 300, have the lowest proper motions in the survey, moving only  $\sim 225$  mas and  $\sim 286$  mas, respectively, between their 2003 first epoch and 2005 second epoch images. This motion is only  $\sim 1.7$  and  $\sim 2.0$  times larger than the rms of the magnitude of the motion of all the point sources in the fields of WD 0148 + 467 and WD 1134 + 300, respectively, with  $21.5 < J < 22.5$  mag. In addition, their first epoch images were degraded by 60 Hz interference. Due to the combination of the very low proper motions of these white dwarfs and the presence of 60 Hz interference, third epoch images are required to clearly distinguish their proper motions from the motions of the background objects in the field.

WD 1633 + 433, WD 1900 + 705 and WD 2246 + 223 all move  $> 450$  mas between their 2003 first epoch and 2004 second epoch images. However, their first epoch images were degraded by 60 Hz interference. In addition, the presence of a streak in the first epoch image of WD 1633 + 433 has most likely decreased the accuracy of the measurement of

**Figure 27.** The motion of the objects between the 2003 first epoch and 2005 second epoch images of WD 0148 + 467. The white dwarf has a magnitude of  $J \sim 13$  mag.**Figure 28.** The motion of the objects between the first epoch and second epoch images of WD 1134 + 300. The white dwarf has a magnitude of  $J \sim 13$  mag.

the motion of the faintest objects in the field. Again, third epoch images, without the presence of any interference, are required.

Using the 2008 third epoch image of WD 2007 - 219, the necessary minimum baseline to reliably distinguish real common proper motion companions from non-moving background objects was determined. For the faintest (and by implication, the most interesting) sources ( $\text{SNR} \lesssim 10$ , corresponding to  $J \gtrsim 22$  for the majority of the images in the DODO survey) the white dwarf needs to have moved at least 4 pixels ( $\sim 470$  mas for the *NIRI* data) between the two epoch images to conclusively rule out non-moving outliers at this magnitude.

The cumulative completeness limits, in terms of mass and effective temperature, and the corresponding range of projected physical separations over which these limits apply have been determined for all 23 equatorial and northern hemisphere white dwarfs discussed in this paper (Figures 31, 32, 33, 34).

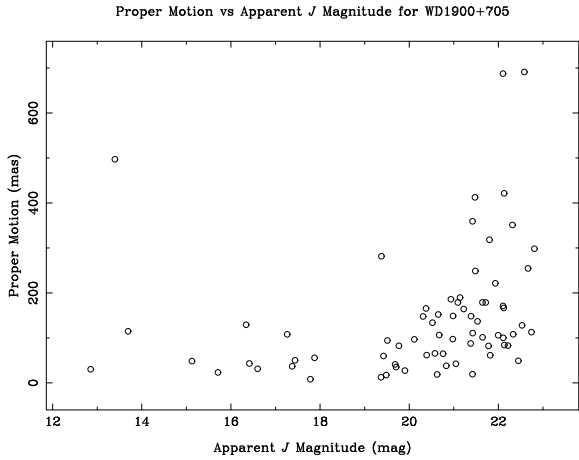


**Figure 29.** The motion of the objects between the first epoch and second epoch images of WD 1900 + 705. The white dwarf has a magnitude of  $J \sim 13.5$  mag.

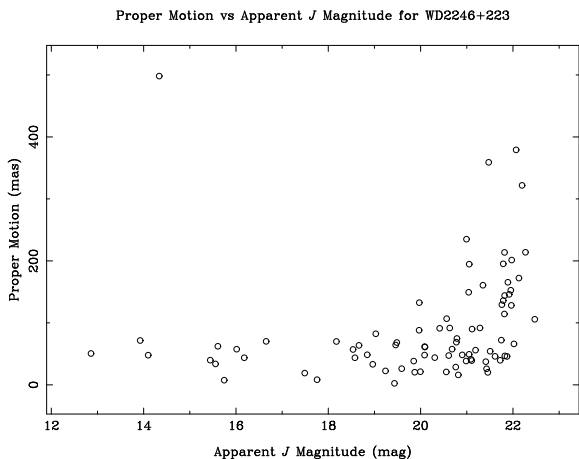


**Figure 30.** The motion of the objects between the first epoch and second epoch images of WD 2246 + 223. The white dwarf has a magnitude of  $J \sim 14.3$  mag.

From these results, tentative conclusions regarding the frequency of substellar and planetary mass companions to white dwarfs and their main sequence progenitors at wide separations can be made (we recognise that the DODO survey contains a relatively small number of targets). These conclusions assume that no common proper motion companions are confirmed around the 5 white dwarfs requiring a third epoch image and include the non-detection of a companion around WD 0046+051 (Burleigh et al. 2008). Firstly, using the 90% completeness limits, the DODO survey can detect companions with effective temperatures  $\gtrsim 500$  K around *all* targets. This is significantly below the currently coolest known brown dwarfs, ULAS J003402.77 – 005206.7 (Warren et al. 2007) and CFBDS J005910.90 – 011401.3 (Delorme et al. 2008), which have effective temperatures of  $600 < T_{\text{eff}} < 700$  K and spectral types of T8.5. In fact, these observations probe well into the hypothetical Y dwarf regime or at least into a significant extension of the T dwarf sequence (Kirkpatrick 2005). Therefore, we suggest

that  $\lesssim 5\%$  of white dwarfs have L, T and sub-T8.5 (Y?) substellar companions with effective temperatures  $\gtrsim 500$  K between projected physical separations of 60 – 200 AU, although for many fields this applies to smaller ( $\sim 13$  AU for WD 0046 + 051; Burleigh et al. 2008) and larger ( $\sim 800$  AU) projected physical separations. This corresponds to projected physical separations around their main sequence progenitors ( $1.5 - 8 M_{\odot}$ , i.e., spectral types F5–B5) of 20 – 45 AU, although again for many fields these limits apply to smaller ( $\sim 3$  AU for WD 0046+051; Burleigh et al. 2008) and larger ( $\sim 200$  AU) projected physical separations. For the same range of projected physical separations stated above and using the 50% completeness limits, we suggest that  $\lesssim 8\%$  of white dwarfs and their main sequence progenitors have companions with masses above the deuterium burning limit ( $\sim 13 M_{\text{Jup}}$ ), while  $\lesssim 9\%$  have companions with masses  $\gtrsim 10 M_{\text{Jup}}$ .

These results can be compared to the results from other imaging surveys for wide substellar and planetary mass companions to white dwarfs and main sequence stars (Table 5). In particular, our results are consistent with those of McCarthy & Zuckerman (2004) and Lafrenière et al. (2007). We note the recent claims of the directly imaged planetary mass companions to Fomalhaut (Kalas et al. 2008) and HR8799 (Marois et al. 2008) and await the statistical analyses of those surveys for comparison with the DODO survey results. The DODO survey results can also be compared to complimentary recent MIR searches for *unresolved* substellar and planetary mass companions to white dwarfs (e.g., Mullally et al. 2007). A recent MIR photometric survey of 27 white dwarfs using the Spitzer Space Telescope and IRAC was sensitive to the entire known T dwarf sequence (Farihi et al. 2008). Their observations place similar limits ( $\lesssim 4\%$ ) on the frequency of such companions to white dwarfs, but at smaller separations (with some overlap) compared to the DODO survey.

At this stage, we prefer to refrain from speculating on the reasons for the negative results so far. For example, from radial velocity measurements of evolved giant stars, Lovis & Mayor (2007) estimate that at least 3% of stars with  $M \gtrsim 1.8 M_{\odot}$  host  $M_p \sin i > 5 M_{\text{Jup}}$  companions, including brown dwarfs. Therefore, it is not unreasonable to have expected that at least one of our target white dwarfs would have had a detectable companion. It may simply be a case of observing more targets.

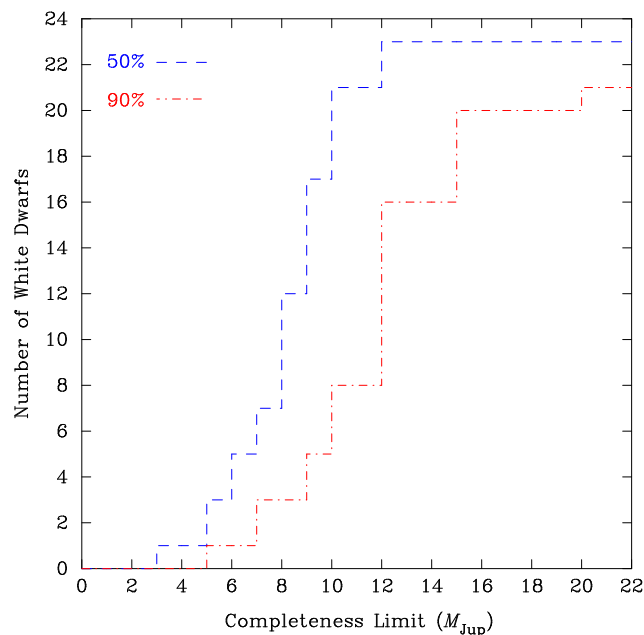
A more substantial comparison with similar surveys, along with a more thorough statistical analysis of our results, will be presented in a forthcoming paper on the southern hemisphere white dwarfs in the DODO survey.

## 8 ACKNOWLEDGEMENTS

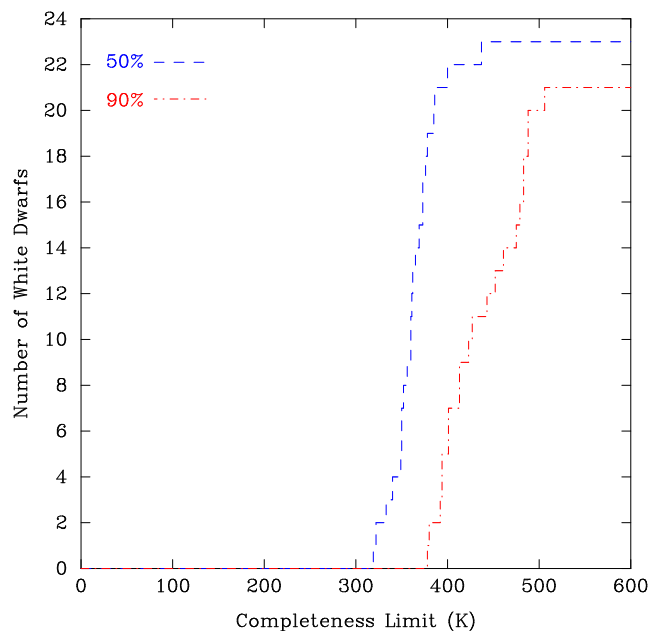
EH acknowledges the support of a PPARC Postgraduate Studentship. MRB acknowledges the support of a STFC Advanced Fellowship. Based on observations obtained at the Gemini Observatory, which is operated by the Association of Universities for Research in Astronomy, Inc., under a cooperative agreement with the NSF on behalf of the Gemini partnership: the National Science Foundation (United States), the Particle Physics and Astronomy Research Council (United Kingdom), the National Research

**Table 5.** Recent imaging searches for wide companions

Survey	Targets	Number of Targets	Limit [ $M_{\text{Jup}}$ ]	Separation [AU]	Frequency of Companions
McCarthy & Zuckerman (2004)	G K M	102	> 12	75 - 300	1% $\pm$ 1%
		178	> 30	140 - 1200	0.7% $\pm$ 0.7%
Farihi et al. (2005)	White Dwarfs	261	> 52	75 - 300	< 3%
		86	> 21	100 - 5000	< 0.5%
Allen et al. (2007)	M7-L8	132	> 52	50 - 1100	< 0.5%
Lafrenière et al. (2007)	F G K M	85	13-40	40 - 1000	< 2.3%
Nielsen et al. (2008)	A F G K M	60	> 4	25 - 250	< 5.6%
				20 - 100	< 20%

**Figure 31.** The cumulative completeness limit, in terms of companion mass, for the 23 equatorial and northern hemisphere white dwarfs in the DODO survey. The red dotted-dashed line indicates the frequency of the completeness limit in  $M_{\text{Jup}}$  at which 90% of companions with that mass could be detected, while the blue dashed line indicates the completeness limit in  $M_{\text{Jup}}$  at which 50% of companions with that mass could be detected.

Council (Canada), CONICYT (Chile), the Australian Research Council (Australia), CNPq (Brazil) and CONICET (Argentina). IRAF is distributed by the National Optical Astronomy Observatories, which are operated by the Association of Universities for Research in Astronomy, Inc., under cooperative agreement with the National Science Foundation. This publication makes use of data products from the Two Micron All Sky Survey, which is a joint project of the University of Massachusetts and the Infrared Processing and Analysis Center/California Institute of Technology, funded by the National Aeronautics and Space Administration and the National Science Foundation. This research has made use of the SIMBAD database, operated at CDS, Strasbourg, France.

**Figure 32.** The cumulative completeness limit, in terms of companion temperature, for the 23 equatorial and northern hemisphere white dwarfs in the DODO survey. The red dotted-dashed line indicates the frequency of the completeness limit in Kelvin at which 90% of companions with that temperature could be detected, while the blue dashed line indicates the completeness limit in Kelvin at which 50% of companions with that temperature could be detected.

## REFERENCES

- Allen P. R., Koerner D. W., McElwain M. W., Cruz K. L., Reid I. N., 2007, *AJ*, 133, 971  
 Bakos G. Á., Sahu K. C., Németh P., 2002, *ApJS*, 141, 187  
 Baraffe I., Chabrier G., Barman T., 2008, *A&A*, 482, 315  
 Baraffe I., Chabrier G., Barman T. S., Allard F., Hauschildt P. H., 2003, *A&A*, 402, 701  
 Becklin E. E., Farihi J., Jura M., Song I., Weinberger A. J., Zuckerman B., 2005, *ApJ*, 632, L119  
 Becklin E. E., Zuckerman B., 1988, *Nature*, 336, 656  
 Bergeron P., Leggett S. K., Ruiz M. T., 2001, *ApJS*, 133, 413  
 Bergeron P., Saffer R. A., Liebert J., 1992, *ApJ*, 394, 228  
 Bertin E., Arnouts S., 1996, *A&AS*, 117, 393  
 Brinkworth C. S., Marsh T. R., Morales-Rueda L., Maxted

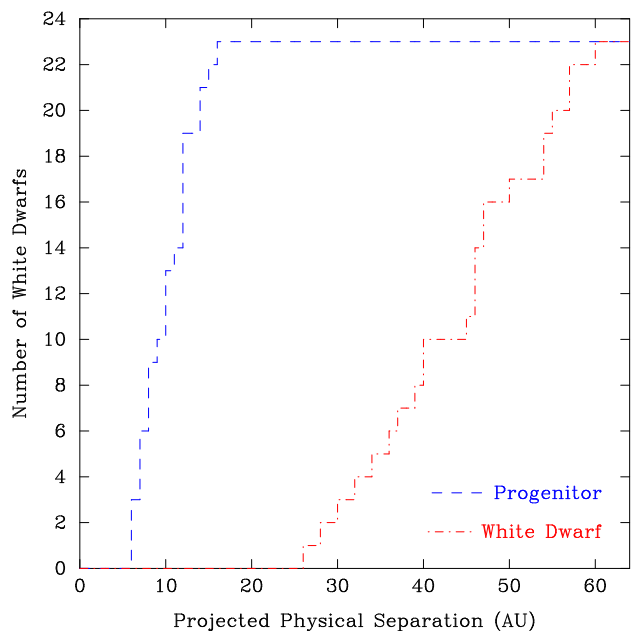


**Figure 33.** The cumulative minimum projected physical separations for the 23 equatorial and northern hemisphere white dwarfs in the DODO survey. The red dotted–dashed line indicates the minimum projected physical separations in AU at which a companion could be found around each white dwarf. The blue dashed line indicates the minimum projected physical separations in AU at which a companion could be found around the main sequence progenitor.

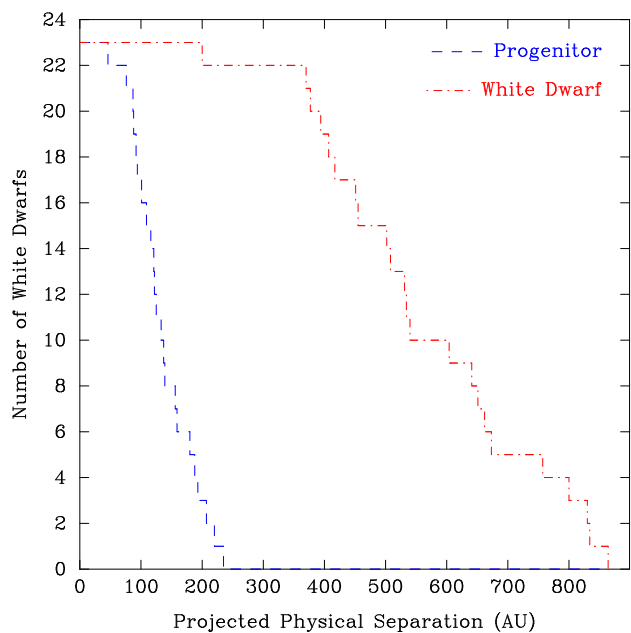


**Figure 34.** The cumulative maximum projected physical separations for the 23 equatorial and northern hemisphere white dwarfs in the DODO survey. The red dotted–dashed line indicates the maximum projected physical separations in AU at which a companion could be found around each white dwarf. The blue dashed line indicates the maximum projected physical separations in AU at which a companion could be found around the main sequence progenitor.

- P. F. L., Burleigh M. R., Good S. A., 2005, *MNRAS*, 357, 333
- Burleigh M., Hogan E., Clarke F., 2006, in Whitelock P., Dennefeld M., Leibundgut B., eds, *The Scientific Requirements for Extremely Large Telescopes Vol. 232 of IAU Symposium, Direct imaging searches for planets around white dwarf stars*. pp 344–349
- Burleigh M. R., Clarke F. J., Hodgkin S. T., 2002, *MNRAS*, 331, L41
- Burleigh M. R., Clarke F. J., Hogan E., Brinkworth C. S., Bergeron P., Dufour P., Dobbie P. D., Levan A. J., Hodgkin S. T., Hoard D. W., Wachter S., 2008, *MNRAS*, pp L35+
- Burleigh M. R., Hogan E., Dobbie P. D., Napiwotzki R., Maxted P. F. L., 2006, *MNRAS*, 373, L55
- Burrows A., Marley M., Hubbard W. B., Lunine J. I., Guillot T., Saumon D., Freedman R., Sudarsky D., Sharp C., 1997, *ApJ*, 491, 856
- Butler R. P., Tinney C. G., Marcy G. W., Jones H. R. A., Penny A. J., Apps K., 2001, *ApJ*, 555, 410
- Casewell S. L., Dobbie P. D., Napiwotzki R., Barstow M. A., Burleigh M. R., Jameson R. F., 2008, *MNRAS*, in press
- Catalán S., Isern J., García-Berro E., Ribas I., Allende Prieto C., Bonanos A. Z., 2008, *A&A*, 477, 213
- Chabrier G., Baraffe I., Leconte J., Gallardo J., barman T., 2008, *ArXiv e-prints*
- Chauvin G., Lagrange A.-M., Dumas C., Zuckerman B., Mouillet D., Song I., Beuzit J.-L., Lowrance P., 2004, *A&A*, 425, L29
- Chauvin G., Lagrange A.-M., Dumas C., Zuckerman B., Mouillet D., Song I., Beuzit J.-L., Lowrance P., 2005, *A&A*, 438, L25
- Chauvin G., Lagrange A.-M., Udry S., Fusco T., Galland F., Naef D., Beuzit J.-L., Mayor M., 2006, *A&A*, 456, 1165
- Chauvin G., Lagrange A.-M., Udry S., Mayor M., 2007, *A&A*, 475, 723
- Chauvin G., Thomson M., Dumas C., Beuzit J.-L., Lowrance P., Fusco T., Lagrange A.-M., Zuckerman B., Mouillet D., 2003, *A&A*, 404, 157
- Clarke F. J., Burleigh M. R., 2004, in Beaulieu J., Lecavelier Des Etangs A., Terquem C., eds, *ASP Conf. Ser. 321: Extrasolar Planets: Today and Tomorrow Imaging Planets around White Dwarfs; First Results*. pp 76–+
- Debes J. H., Ge J., Ftaclas C., 2006, *AJ*, 131, 640
- Debes J. H., Sigurdsson S., 2002, *ApJ*, 572, 556
- Debes J. H., Sigurdsson S., Woodgate B. E., 2005a, *ApJ*, 633, 1168
- Debes J. H., Sigurdsson S., Woodgate B. E., 2005b, *AJ*, 130, 1221
- Delorme P., Delfosse X., Albert L., Artigau E., Forveille T., Reylé C., Allard F., Homeier D., Robin A., Willott C. J., Liu M., Dupuy T., 2008, *ArXiv e-prints*, 802
- Desidera S., Barbieri M., 2007, *A&A*, 462, 345
- Dobbie P. D., Burleigh M. R., Levan A. J., Barstow M. A., Napiwotzki R., Holberg J. B., Hubeny I., Howell S. B., 2005, *MNRAS*, 357, 1049
- Dobbie P. D., Napiwotzki R., Burleigh M. R., Barstow M. A., Boyce D. D., Casewell S. L., Jameson R. F., Hubeny I., Fontaine G., 2006, *MNRAS*, 369, 383
- Ducourant C., Teixeira R., Chauvin G., Daigne G., Le Campion J.-F., Song I., Zuckerman B., 2008, *A&A*, 477,

- L1
- Dufour P., Bergeron P., Fontaine G., 2005, *ApJ*, 627, 404
- Duncan M. J., Lissauer J. J., 1998, *Icarus*, 134, 303
- Farihi J., Becklin E. E., Zuckerman B., 2005, *ApJS*, 161, 394
- Farihi J., Becklin E. E., Zuckerman B., 2008, *ArXiv e-prints*, 804
- Farihi J., Christopher M., 2004, *AJ*, 128, 1868
- Farihi J., Zuckerman B., Becklin E. E., 2008, *ApJ*, 674, 431
- Fontaine G., Bergeron P., Brassard P., 2007, in *Napiwotzki A., Burleigh M. R., eds, Astronomical Society of the Pacific Conference Series Vol. 372 of Astronomical Society of the Pacific Conference Series, G 87-7: A White Dwarf with a Strange Core Composition?*. pp 13–+
- Fontaine G., Brassard P., Bergeron P., 2001, *PASP*, 113, 409
- Galland F., Lagrange A.-M., Udry S., Chelli A., Pepe F., Queloz D., Beuzit J.-L., Mayor M., 2005, *A&A*, 443, 337
- Gänsicke B. T., Marsh T. R., Southworth J., 2007, *MNRAS*, 380, L35
- Gänsicke B. T., Marsh T. R., Southworth J., Rebassamansergas A., 2006, *Science*, 314, 1908
- Gianninas A., Bergeron P., Fontaine G., 2005, *ApJ*, 631, 1100
- Giovannini O., Kepler S. O., Kanaan A., Wood A., Claver C. F., Koester D., 1998, *Baltic Astronomy*, 7, 131
- Graham J. R., Matthews K., Neugebauer G., Soifer B. T., 1990, *ApJ*, 357, 216
- Hatzes A. P., Cochran W. D., Endl M., Guenther E. W., Saar S. H., Walker G. A. H., Yang S., Hartmann M., Esposito M., Paulson D. B., Döllinger M. P., 2006, *A&A*, 457, 335
- Hatzes A. P., Guenther E. W., Endl M., Cochran W. D., Döllinger M. P., Bedalov A., 2005, *A&A*, 437, 743
- Hodapp K. W., Jensen J. B., Irwin E. M., Yamada H., Chung R., Fletcher K., Robertson L., Hora J. L., Simons D. A., Mays W., Nolan R., Bec M., Merrill M., Fowler A. M., 2003, *PASP*, 115, 1388
- Hogan E., Burleigh M. R., Clarke F. J., 2007, in *Napiwotzki A., Burleigh M. R., eds, Astronomical Society of the Pacific Conference Series Vol. 372 of Astronomical Society of the Pacific Conference Series, The DODO Survey: Imaging Planets around White Dwarfs*. pp 349–+
- Holberg J. B., Oswalt T. D., Sion E. M., 2002, *ApJ*, 571, 512
- Jeans J. H., 1924, *MNRAS*, 85, 2
- Johnson J. A., Butler R. P., Marcy G. W., Fischer D. A., Vogt S. S., Wright J. T., Peek K. M. G., 2007, *ApJ*, 670, 833
- Jura M., 2003, *ApJ*, 584, L91
- Jura M., 2006, *ApJ*, 653, 613
- Jura M., Farihi J., Zuckerman B., 2007, *ApJ*, 663, 1285
- Kalas P., Graham J. R., Chiang E., Fitzgerald M. P., Clampin M., Kite E. S., Stapelfeldt K., Marois C., Krist J., 2008, *ArXiv e-prints*
- Kalirai J. S., Hansen B. M. S., Kelson D. D., Reitzel D. B., Rich R. M., Richer H. B., 2008, *ApJ*, 676, 594
- Kilic M., Redfield S., 2007, *ApJ*, 660, 641
- Kilic M., von Hippel T., Leggett S. K., Winget D. E., 2005, *ApJ*, 632, L115
- Kilic M., von Hippel T., Leggett S. K., Winget D. E., 2006, *ApJ*, 646, 474
- Kirkpatrick J. D., 2005, *ARA&A*, 43, 195
- Koester D., Napiwotzki R., Christlieb N., Drechsel H., Hagen H.-J., Heber U., Homeier D., Karl C., Leibundgut B., Moehler S., Nelemans G., Pauli E.-M., Reimers D., Renzini A., Yungelson L., 2001, *A&A*, 378, 556
- Lafrenière D., Doyon R., Marois C., Nadeau D., Oppenheimer B. R., Roche P. F., Rigaut F., Graham J. R., Jayawardhana R., Johnstone D., Kalas P. G., Macintosh B., Racine R., 2007, *ApJ*, 670, 1367
- Lagrange A.-M., Beust H., Udry S., Chauvin G., Mayor M., 2006, *A&A*, 459, 955
- Liebert J., Bergeron P., Holberg J. B., 2005, *VizieR Online Data Catalog*, 215, 60047
- Lodato G., Delgado-Donate E., Clarke C. J., 2005, *MNRAS*, 364, L91
- Lovis C., Mayor M., 2007, *A&A*, 472, 657
- Marois C., Macintosh B., Barman T., Zuckerman B., Song I., Patience J., Lafreniere D., Doyon R., 2008, *ArXiv e-prints*
- Mathews G. J., Suh I.-S., O’Gorman B., Lan N. Q., Zech W., Otsuki K., Weber F., 2006, *Journal of Physics G Nuclear Physics*, 32, 747
- Maxted P. F. L., Napiwotzki R., Dobbie P. D., Burleigh M. R., 2006, *Nature*, 442, 543
- Mayor M., Udry S., Naef D., Pepe F., Queloz D., Santos N. C., Burnet M., 2004, *A&A*, 415, 391
- McCarthy C., Zuckerman B., 2004, *AJ*, 127, 2871
- Monteiro H., Jao W.-C., Henry T., Subasavage J., Beaulieu T., 2006, *ApJ*, 638, 446
- Mugrauer M., Neuhäuser R., 2005, *MNRAS*, 361, L15
- Mugrauer M., Neuhäuser R., Mazeh T., 2007, *A&A*, 469, 755
- Mullally F., Kilic M., Reach W. T., Kuchner M. J., von Hippel T., Burrows A., Winget D. E., 2007, *ApJS*, 171, 206
- Mullally F., Winget D. E., Degennaro S., Jeffery E., Thompson S. E., Chandler D., Kepler S. O., 2008, *ApJ*, 676, 573
- Neuhäuser R., Guenther E. W., Alves J., Huélamo N., Ott T., Eckart A., 2003, *Astronomische Nachrichten*, 324, 535
- Nielsen E. L., Close L. M., Biller B. A., Masciadri E., Lenzen R., 2008, *ApJ*, 674, 466
- Perryman M. A. C., et al., 1997, *A&A*, 323, L49
- Pinfeld D. J., Jones H. R. A., Lucas P. W., Kendall T. R., Folkes S. L., Day-Jones A. C., Chappelle R. J., Steele I. A., 2006, *MNRAS*, 368, 1281
- Poveda A., Herrera M. A., Allen C., Cordero G., Lavalley C., 1994, *Revista Mexicana de Astronomia y Astrofisica*, 28, 43
- Probst R. G., 1983, *ApJS*, 53, 335
- Provencal J. L., Shipman H. L., Hog E., Thejll P., 1998, *ApJ*, 494, 759
- Queloz D., Mayor M., Weber L., Blécha A., Burnet M., Confino B., Naef D., Pepe F., Santos N., Udry S., 2000, *A&A*, 354, 99
- Raghavan D., Henry T. J., Mason B. D., Subasavage J. P., Jao W.-C., Beaulieu T. D., Hambly N. C., 2006, *ApJ*, 646, 523
- Reach W. T., Kuchner M. J., von Hippel T., Burrows A., Mullally F., Kilic M., Winget D. E., 2005, *ApJ*, 635, L161
- Reffert S., Quirrenbach A., Mitchell D. S., Albrecht S., Hekker S., Fischer D. A., Marcy G. W., Butler R. P.,



- 2006, ApJ, 652, 661
- Salim S., Gould A., 2003, ApJ, 582, 1011
- Setiawan J., Rodmann J., da Silva L., Hatzes A. P., Pasquini L., von der Lühe O., de Medeiros J. R., Döllinger M. P., Girardi L., 2005, A&A, 437, L31
- Shipman H. L., 1986, in Kafatos M. C., Harrington R. S., Maran S. P., eds, *Astrophysics of Brown Dwarfs An unsuccessful search for brown dwarf companions to white dwarf stars*. pp 71–75
- Silvotti R., Schuh S., Janulis R., et al., 2007, Nature, 449, 189
- Skrutskie M. F., Cutri R. M., Stiening R., et al., 2006, AJ, 131, 1163
- Tody D., 1986, in Crawford D. L., ed., *Instrumentation in astronomy VI; Proceedings of the Meeting, Tucson, AZ, Mar. 4-8, 1986. Part 2 (A87-36376 15-35)*. Bellingham, WA, Society of Photo-Optical Instrumentation Engineers, 1986, p. 733. The IRAF Data Reduction and Analysis System. pp 733–+
- Tokunaga A. T., Becklin E. E., Zuckerman B., 1990, ApJ, 358, L21
- van Altena W. F., Lee J. T., Hoffleit D., 1995, *VizieR Online Data Catalog*, 1174, 0
- Villaver E., Livio M., 2007, ApJ, 661, 1192
- von Hippel T., Kuchner M. J., Kilic M., Mullally F., Reach W. T., 2007, ApJ, 662, 544
- Warren S. J., Mortlock D. J., Leggett S. K., et al., 2007, MNRAS, 381, 1400
- Wegner G., 1973, MNRAS, 165, 271
- Wickramasinghe D. T., Ferrario L., 2000, PASP, 112, 873
- Wood M. A., 1992, ApJ, 386, 539
- Zuckerman B., Becklin E. E., 1987a, ApJ, 319, L99
- Zuckerman B., Becklin E. E., 1987b, Nature, 330, 138
- Zuckerman B., Song I., 2008, ArXiv e-prints